

# Evaluation of WRF and CHIMERE models for the simulation of PM<sub>2.5</sub> in large East African urban conurbations.

Andrea Mazzeo<sup>1,2</sup>, Michael Burrow<sup>1</sup>, Andrew Quinn<sup>1</sup>, Eloise A. Marais<sup>3</sup>, Ajit Singh<sup>2</sup>, David Ng'ang'a<sup>4</sup>, Michael J. Gatari<sup>4</sup>, and Francis D. Pope<sup>2</sup>

1. School of Civil Engineering, University of Birmingham, Birmingham UK

2. School of Geography Earth and Environmental Sciences – GEES, University of Birmingham, Birmingham UK

3. Department of Geography, University College London, London, UK.

4. Institute of Nuclear Science and Technology, University of Nairobi, Nairobi, Kenya

Correspondence to Andrea Mazzeo ([a.mazzeo@bham.ac.uk](mailto:a.mazzeo@bham.ac.uk))

**Abstract:** *Urban conurbations of East Africa are affected by harmful levels of air pollution. The paucity of local air quality networks and the absence of capacity to forecast air quality make it difficult to quantify the real level of air pollution in this area. The chemistry-transport model CHIMERE has been used along with the meteorological model WRF to run simulations at high spatial resolution of hourly concentrations of Particulate Matter PM<sub>2.5</sub> for three East African urban conurbations: Addis Ababa in Ethiopia, Nairobi in Kenya, and Kampala in Uganda. Two existing emission inventories were combined to test the performance of CHIMERE as an air quality tool for a target monthly period of 2017 and the results compared against observed data from urban, roadside, and rural sites. The results show that the model is able to reproduce hourly and daily temporal variability of aerosol concentrations close to observations in urban, roadside and in rural environments. CHIMERE's performance as a tool for managing air quality was also assessed. The analysis demonstrated that despite the absence of high-resolution data and up-to-date biogenic and anthropogenic emissions, the model was able to reproduce 66 – 99% of the daily PM<sub>2.5</sub> exceedances above the WHO 24-hour mean PM<sub>2.5</sub> guideline (25  $\mu\text{g m}^{-3}$ ) in the three cities. An analysis of the 24-hour average levels of PM<sub>2.5</sub> was also carried out for 17 constituencies in the vicinity of Nairobi. This showed that 47% of the constituencies in the area exhibited a low air quality index for PM<sub>2.5</sub> in the unhealthy category for human health exposing between 10,000 to 30,000 people/km<sup>2</sup> to harmful levels of air contamination.*

**Keywords:** Air quality, East Africa, Particulate Matter, Anthropogenic emissions, numerical modelling, Air Quality Index

## 1 Introduction

The world's population has grown rapidly by 1 billion people in the last 12 years, reaching 7.9 billion in 2021. Future projections suggest a continuing annual increase of 1.8 %, meaning the global population will reach 8.5 billion by 2030, 9.7 by 2050, and 11.2 by 2100 (WPP, 2015). The African continent is predicted to have the fastest growing population rate in the world, and it is projected to double between 2010 and 2050, surpassing two billion (WPP, 2011). In addition to this a 60 % increase in population has been predicted by 2050, specifically in urban areas (WPP, 2012).

41

42 Population in Sub-Saharan East African (SSEA) countries have increased drastically from 1991 to 2019. In that  
43 period of time and according to data from the World Bank database (WB, 2022), the Kenyan population grew  
44 from 24 to 52 million, the Ugandan population from 17 to 44 million and the Ethiopian population from 50 to 112  
45 million. These increases in population were accompanied by a similar rate of increase in road transport, industrial  
46 activities and in the use of solid fuels (e.g., woods, charcoal, and agricultural residues) for cooking purposes in  
47 urban areas (Bockarie et al., 2020;Marais et al., 2019).

48

49 As a result of these population increases, air quality of the urban areas of these countries, historically influenced  
50 by the large presence of seasonal burning biomass emissions (Haywood et al., 2008;Lacaux, 1995;Liousse et al.,  
51 2010;Thompson A. M., 2001), is progressively degrading (Marais and Wiedinmyer, 2016). This, in combination  
52 with the expanding urban population, has greatly increased the exposure of citizens to harmful Particulate Matter  
53 (PM) pollution with an aerodynamic diameter smaller than 10 and 2.5  $\mu\text{m}$  ( $\text{PM}_{10}$  and  $\text{PM}_{2.5}$ , respectively) (Gatari  
54 et al., 2019;Kinney et al., 2011;Li et al., 2017;UN-Habitat, 2017).

55

56 Several diseases have been attributed to PM exposure in SSEA, including cardiovascular and cardiopulmonary  
57 diseases, cancers, and respiratory deep infections (Dalal et al., 2011;Mbewu, 2006;Parkin et al., 2008). In 2012,  
58 the World Health Organization (WHO) estimated that in 2012 176,000 deaths in SSEA were directly connected  
59 to air pollution (WHO, 2012). Modelling studies have also found that exposure to outdoor air pollution has led to  
60 626,000 disability-adjusted life per year (DALYs) in SSEA alone (Amegah and Agyei-Mensah, 2017),  
61 highlighting that these numbers could be much higher considering the limited amount of air quality data emanating  
62 from the region that are available for research purposes.

63

64 Considering the likely severe impacts of air pollution on human health in SSEA, the research interest in  
65 understanding air pollution trends in East Africa has increased in recent years. Many researchers have analysed  
66 the levels of contamination by short-term measurement campaigns (Amegah and Agyei-Mensah, 2017;deSouza  
67 P., 2017;Egondi et al., 2013;Gaita et al., 2014;Gatari et al., 2019;Kume, 2010;Ngo et al., 2015;Pope et al.,  
68 2018;Schwander et al., 2014;Vliet, 2007;Singh et al., 2021). Other studies observed annual average  $\text{PM}_{2.5}$   
69 concentrations in the order of 100  $\mu\text{g m}^{-3}$  quantified in a small number of urban areas of SSEA (Brauer et al.,  
70 2012). These levels are about four times higher than the 24-hour average and ten times higher than the annual  
71 average WHO guidelines for  $\text{PM}_{2.5}$  (Avis W. and Khaemba W., 2018;WHO, 2016) and underline that air pollution  
72 is a serious problem in this area of the world. A recent study by Singh et al. (2020), using visibility as a proxy for  
73 PM, showed that air quality in Addis Ababa, Kampala and Nairobi has degraded alarmingly over the last 4  
74 decades.

75

76 The lack of long-term air quality monitoring networks in many African countries have made it difficult to have  
77 reliable long-term air quality data (Petkova, 2013;Pope et al., 2018;Singh et al., 2020) and still little is known  
78 about the levels of air contamination in large urban conurbations (Peña, 2017). The paucity and sometimes  
79 complete absence of reliable data on air pollution levels makes it difficult to quantify the magnitude of the  
80 problem. Consequently, it is difficult for local and national authorities to plan possible improvement measures for

81 the mitigation of anthropogenic emissions. Even if important steps forward have been made to improve the  
82 knowledge relative to anthropogenic emissions and emission inventories for Africa used for numerical simulations  
83 and forecasts of air quality (Assamoi and Liousse, 2010;Liousse, 2014;Marais and Wiedinmyer, 2016) the lack of  
84 surface observations to validate the emission magnitude and the simulated concentrations make these inventories  
85 susceptible of large error.

86

87 In this work we test a meteorological and a chemistry-transport model (CTM) to simulate the hourly urban and  
88 rural levels of PM<sub>2.5</sub> in three SSEA urban conurbations during a monthly period of 2017. We present the results  
89 of the validation of both models for the capital cities of Kenya, (Nairobi), Ethiopia (Addis Ababa) and Uganda  
90 (Kampala) against observation data. For Nairobi, we compare model outputs with observations from rural and  
91 roadside sites observations collected during the “A Systems approach to Air Pollution in East Africa” research  
92 project (ASAP-East Africa - [www.asap-eastafrica.com](http://www.asap-eastafrica.com), hereafter called ASAP) (Pope et al., 2018). For Addis  
93 Ababa and Kampala, the model was validated using hourly observations of PM<sub>2.5</sub> collected by the respective U.S.  
94 Embassies.

95

96 Moreover, we assess the suitability of the CTM as a decision support tool for policy makers to plan possible  
97 mitigation policies oriented to quantify the real level of air pollution in urban areas and quantify the human  
98 exposure to PM<sub>2.5</sub>. Specifically, in terms of the accuracy of the model in estimating the daily WHO threshold limit  
99 exceedances of PM<sub>2.5</sub> in the three urban conurbations. Finally, for the particular case of Nairobi, we evaluate the  
100 average air quality indices by local constituency for the whole analysed period giving a new insight of the real  
101 level of air contamination in Nairobi to the general public and the relative population exposed to harmful level of  
102 air contamination.

103

## 104 **2 Material and Methods**

105

106 The meteorological and chemistry-transport models used in this work have been configured to simulate hourly  
107 weather parameters and concentrations of PM<sub>2.5</sub> using available input data for the simulations and observations  
108 from the real world for the validation. The availability of the observations for the validation of both models comes  
109 from different providers, have different frequency in time and, in the case of PM<sub>2.5</sub> observations, come from  
110 different environments (rural, urban, roadside sites). No vertical observations were available for the validation of  
111 both models.

112

### 113 **2.1 Meteorological model WRF**

114

115 The Weather Research and Forecasting (WRF) model is a numerical model for weather predictions and  
116 atmospheric simulations and is used commercially and for research purposes, including by the US National  
117 Oceanic and Atmospheric Administration (Powers, 2017;Skamarock, 2008).

118

119 WRF was used to drive the meteorology for CHIMERE using three geographical domains at different resolutions  
120 (from 18×18 km to 2×2 km) vertically divided into 30 levels, nine of which are below 1500 m. The first external

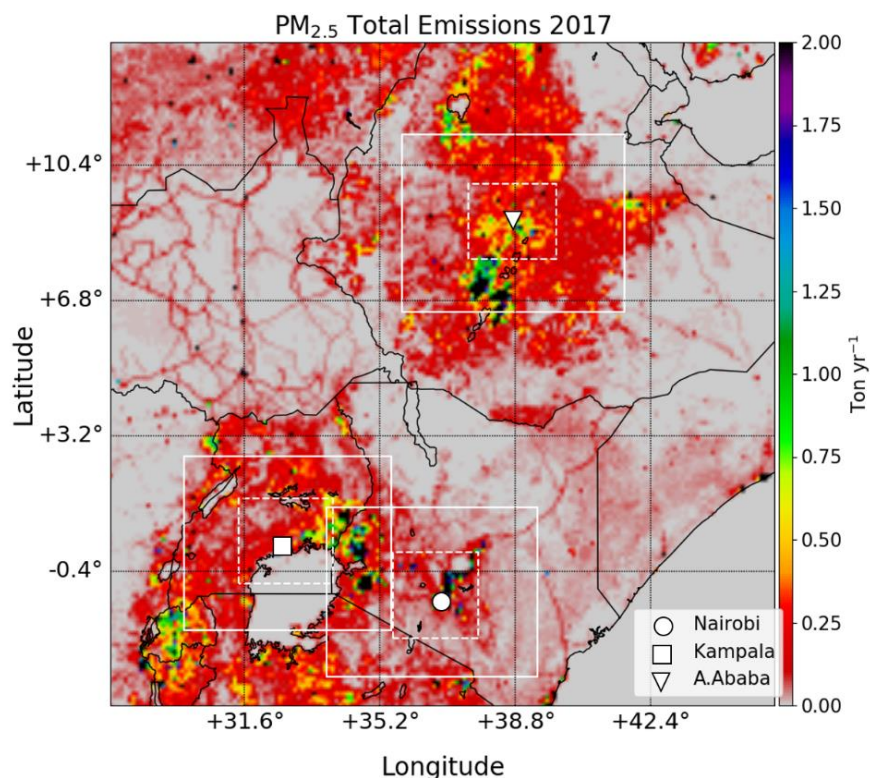
121 domain has a spatial resolution of  $18 \times 18$  km (Figure 1), with three nested domains at a resolution of  $6 \times 6$  km  
122 centred on the three countries of interest (Figure 1, white squares). Three further nested domains with a resolution  
123 of  $2 \times 2$  km centred on Addis Ababa, Kampala, and Nairobi (Figure 1, white dashed squares, and Figure 3a, b, c)  
124 are the focus of the analysis.

125

126 The configuration adopted for the WRF simulations has been chosen according to previous works made on East  
127 Africa (Kerandi et al., 2016; Kerandi et al., 2017; Pohl et al., 2011) and is summarized in Table 1. The Yonsei  
128 University Scheme (YSU - (Hong S., 2006)) was chosen to represent the Planetary Boundary Layer while the  
129 Community Atmosphere Model (CAM - (Collins, 2004)) was used for the long and short-wave radiation scheme.  
130 Initial and boundary conditions for the external coarse domain at  $18 \times 18$  km were obtained from the NCEP FNL  
131 (Final) Operational Global Analysis data (Wu, 2002). Boundary condition for the first ( $6 \times 6$  km) and second ( $2 \times 2$   
132 km) nest domains were taken from the respective parent domains using the two-way-nesting approach. The  
133 process enables the lateral conditions for the internal domains to be calculated from the outputs of the respective  
134 parent domains at lower resolution at every time step of the simulation.

135

136 The land use option chosen for the simulations was NOAH (Tewari, 2004) while the WRF Single-moment 3-  
137 class Scheme (WSM3) for clouds and ice proposed by Hong S. (2004) was chosen for the reproduction of the  
138 microphysical processes in WRF.



139

140 **Figure 1:** Spatial distribution of the  $PM_{2.5}$  emissions from DICE-EDGAR merged emission inventory for East Africa for the  
141 WRF domain at  $18 \times 18$  km of resolution. The continuous white lines show the location of the first nested domain at  $6 \times 6$  km of  
142 resolution used in WRF-CHIMERE. The dashed white squares give the locations of the second nested domains at  $2 \times 2$  km  
143 centred on Addis Ababa (Ethiopia, white triangle), Kampala (Uganda, white square) and Nairobi (Kenya, white circle) used  
144 for WRF-CHIMERE.

145

## 146 2.2 The CHIMERE Chemistry Transport model

147

148 CHIMERE, version 2017r4 (Mailler et al., 2017), is a Eulerian numerical model for reproducing three-  
149 dimensional gas-phase chemistry and aerosols processes of formation, dispersion, wet and dry deposition over a  
150 defined domain with flexible spatial resolutions. CHIMERE has been used for a number of comparative research  
151 studies of Ozone and particulate matter PM<sub>10</sub> from the continental scale, (Bessagnet et al., 2016; Zyryanov et al.,  
152 2012) to the urban scale (van Loon et al., 2007; Vautard et al., 2007; Mazzeo et al., 2018). Furthermore, the model  
153 has been used for event analysis, scenario studies (Markakis et al., 2015; Trewthella et al., 2019), forecasts, and  
154 impact studies of the effects of air pollution on health (Valari and Menut, 2010) and vegetation (Anav et al., 2011).  
155 The authors highlight that the version of CHIMERE adopted is the 2017r4, the most recent available at the time  
156 when the present work was realized.

157

158 CHIMERE model has been used to simulate the first nested domains at 6×6 km and the second nested domains at  
159 2×2 km of spatial resolution. The configuration adopted in this work uses initial and boundary conditions from  
160 the global three-dimensional chemistry-transport model (LMDz-INCA, Hauglustaine et al. (2004)), both for  
161 gaseous pollutants and for aerosols for the most external domain at 6×6 km of resolution while for the most  
162 internal domains at 2×2 km of resolution, the boundary conditions are calculated from model outputs of the parent  
163 domains. The complete chemical mechanism used for all the simulations was SAPRC-07-A (Carter, 2010) which  
164 can describe more than 275 reactions of 85 species. SAPRC-07-A is the most recent chemical mechanism  
165 available for CHIMERE version 2017r4.

166

167 Horizontal and vertical diffusion is calculated using the approach suggested by Van Leer (1979) and the  
168 thermodynamic equilibrium ISORROPIA model (Nenes, 1998) is used for the particle/gases partitioning of semi-  
169 volatile inorganic gases. The model permits calculation of the thermodynamical equilibrium between sulphates,  
170 nitrates, ammonium, sodium, chloride and water dependent upon temperature and relative humidity data.

171

172 Dry and wet deposition is calculated in CHIMERE. The particle dry deposition velocities are calculated as a  
173 function of particle size and density as well as relevant meteorological variables, including deposition processes,  
174 such as, turbulent transfer, Brownian diffusion, impaction, interception, gravitational settling and particle rebound  
175 (Zhang et al., 2001). Wet deposition is described modelled using a first-order decay equation as described in  
176 Loosmore and Cederwall (2004).

177

178 Radiative transfer processes are accounted in CHIMERE using the Fast-JX model (Wild, 2000; Bian, 2002). Fast-  
179 JX is applied also in other models (Voulgarakis, 2009; Real and Sartelet, 2011; Telford et al., 2013). The photolysis  
180 rates calculated by Fast-JX model are validated both inside the limits of the boundary layer (Barnard, 2004) and  
181 in the free troposphere (Voulgarakis, 2009).

182

183 Secondary organic aerosols (SOAs), including biogenic and anthropogenic precursors, are modelled in CHIMERE  
184 as described by (Pun, 2006). SOAs formation is represented as a single-step oxidation of the precursors,

185 differentiating hydrophilic by hydrophobic SOAs in the partitioning formulation. Finally, biogenic emissions were  
 186 taken in account within CHIMERE using MEGAN model outputs as described by (Guenther, 2006).

187

188 **Table 1:** Main configuration parameters adopted for the modelling system WRF-CHIMERE for all simulations.

<b>WRFv3.9.1 Configuration</b>		
<b>Initial and Boundary conditions</b>	GFS FNL- Reanalysis	<i>Wu (2002)</i>
<b>PBL Parametrization</b>	YSU	<i>Hong S. (2006)</i>
<b>SW/LW Radiation Scheme</b>	CAM	<i>Collins (2004)</i>
<b>Land Use</b>	NOAH	<i>Tewari (2004)</i>
<b>Micro Physics Scheme</b>	WSM3	<i>Hong S. (2006)</i>
<b>Vertical Levels</b>		30
<b>CHIMERE2017r4 Configuration</b>		
<b>Initial and boundary conditions</b>	LMDz-INCA	<i>Hauglustaine et al. (2004)</i>
<b>Anthropogenic Emissions</b>	EDGARv3.4.1 + DICE-Africa	<i>Crippa M. (2018); Marais and Wiedinmyer (2016)</i>
<b>Biogenic Emissions</b>	MEGAN	<i>Guenther (2006)</i>
<b>Gas/Aerosol Partitions</b>	ISORROPIA	<i>Nenes (1998)</i>
<b>Secondary Organic Aerosols</b>	1	<i>Pun (2006)</i>
<b>Radiative Transfer</b>	Fast-JX	<i>Wild (2000); Bian (2002)</i>
<b>Chemistry Mechanism</b>	SAPRC-07-A	<i>Carter (2010)</i>
<b>Horiz. / Vert. Transport scheme</b>	VanLeer	<i>Van Leer (1979)</i>
<b>Vertical Levels</b>		30

189

### 190 2.3 Emission Inventories

191

192 To correctly describe the impact of anthropogenic emissions on urban air quality of Nairobi, Kampala and Addis  
 193 Ababa, industrial and on-grid power generation emissions from the Emissions Database for Global Atmospheric  
 194 Research inventory (hereafter EDGAR, version 3.4.1) (Crippa M., 2018) were combined with non-industrial,  
 195 prominent combustion sources from the Diffusive and Inefficient Emission inventory for Africa (hereafter DICE)  
 196 (Marais and Wiedinmyer, 2016).

197

198 EDGAR is a global inventory developed for year 2012 and DICE is a regional inventory for 2013. DICE includes  
 199 important sources in Africa (e.g., motorcycles, kerosene use, open waste burning, and *ad hoc* oil refining, among  
 200 others) that are absent or misrepresented in global inventories. Both inventories represent the most up-to-date  
 201 anthropogenic emissions available for East Africa at the time of the air quality model was used for this work. Both  
 202 inventories have spatial resolution of  $0.1 \times 0.1^\circ$  and provide annual total of anthropogenic emissions for relevant  
 203 gases and aerosols.

204

205 On one hand, EDGAR provides emissions data for CO, NO, NO<sub>2</sub>, SO<sub>2</sub>, NH<sub>3</sub>, NMVOCs, BC, OC, PM<sub>10</sub> and PM<sub>2.5</sub>  
 206 as annual totals divided by the sector according to the IPCC-1996 classification. All human activities with  
 207 exception of large-scale biomass burning are included in EDGAR (Crippa M., 2018). On the other hand, DICE  
 208 provides emissions from particular diffuse and inefficient combustion emission sources (e.g., road transport,  
 209 residential biofuel use, energy production and charcoal production and use) for gaseous pollutants (CO, NO, NO<sub>2</sub>,  
 210 SO<sub>2</sub>, NH<sub>3</sub>, NMVOCs) and aerosols (BC, OC). Seasonal biomass burning that is considered a large pollution source  
 211 in Africa is included in DICE as comparable emissions of black carbon (BC) and higher emissions of nonmethane

212 volatile organic compounds (NMVOCs). Emissions from DICE were used to provide annual total emissions for  
213 particular emission sources considered to be misrepresented or missing in a global inventory such as EDGAR.

214

215 The preparation of the final emission inventory was carried out in two steps. First, DICE and EDGAR inventories  
216 were merged, by pollutant and by sector, following the approach suggested by Marais and Wiedinmyer (2016).  
217  $PM_{2.5}$  emissions are included in DICE as individual components of organic carbon (OC) and black carbon (BC),  
218 but they need to be expressed as lumped  $PM_{2.5}$  in CHIMERE. Therefore  $PM_{2.5}$  was calculated as the sum of  
219 Organic Carbon (OC - originally present in DICE) multiplied for a conversion factor following Pai et al. (2020)  
220 to represent Organic Aerosols emissions and summed with Black Carbon (BC – originally present in DICE) as  
221 follows:

222

$$223 \quad PM_{2.5} = (OC \times c) + BC \quad \text{Eq. (1)}$$

224

225 Secondly, the emisurf2016 pre-processor of CHIMERE was used to scale the emissions from the original  
226 resolution of  $0.1 \times 0.1^\circ$  (~10 km) to the final resolution of each domain simulated ( $6 \times 6$  and  $2 \times 2$  km) using  
227 population density data provided from the Socioeconomic Data and Application Centre (SEDAC)  
228 (<http://sedac.ciesin.columbia.edu/>) as proxy for the spatial distribution. SEDAC provides population density maps  
229 at high resolution ( $1 \times 1$  km) for the years 2010, 2015 and 2020. The SEDAC population density data calculated  
230 for most internal domains at  $2 \times 2$  km (Figure 3a, b, c) suggest for 2010 a total population of 7 million for Nairobi,  
231 4.8 million for Kampala and 4.5 million for Addis Ababa. These totals grow respectively to 8.1, 5.9 and 5.0 million  
232 for 2015 and to 9.4, 7.3 and 5.7 million for 2020. The original SEDAC data were used for a linear extrapolation  
233 of the population density data to the target year 2017 and were used by emisurf2016 for the spatial allocation of  
234 the emissions. Additionally, emisurf2016 permitted to temporally distribute the original total annual emissions  
235 rates according to seasonal, weekly, and daily variation profiles. The resulting merged inventory (hereafter, DICE-  
236 EDGAR) totals by pollutant and sectors for the most external domain at  $18 \times 18$  km of resolution are shown in  
237 Figure 2.

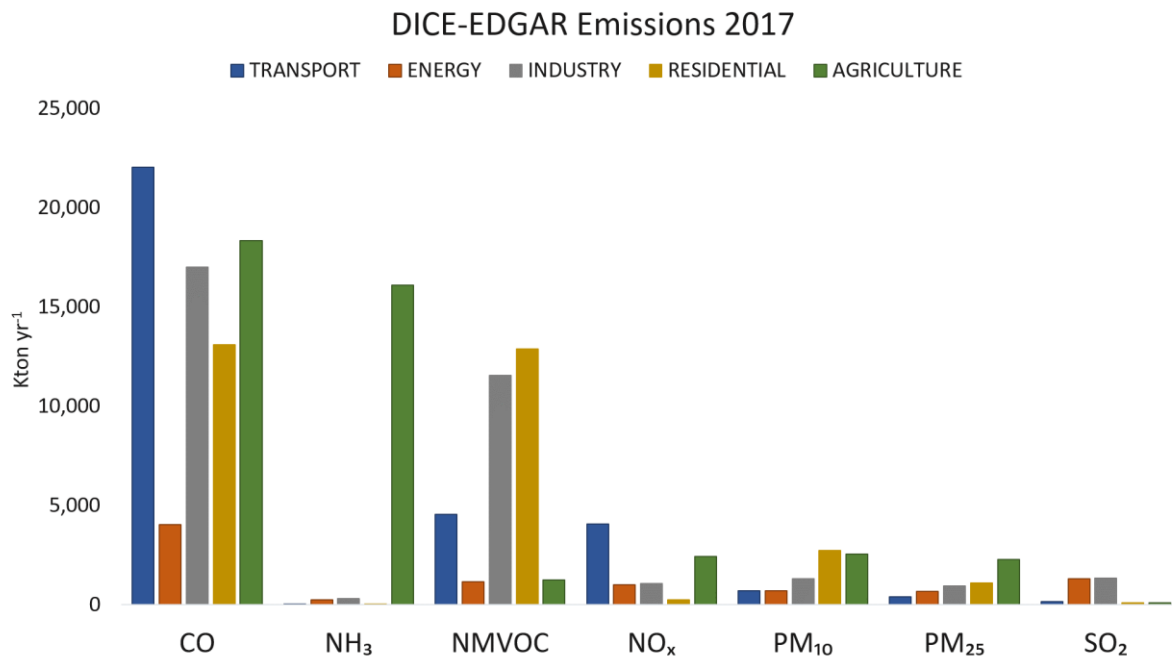
238

239 Biogenic emissions and mineral dust considered in this work have been calculated in-line by CHIMERE. The  
240 former are calculated by MEGAN model outputs as described by Guenther (2006) while the latter are calculated  
241 using the USGS land use database provided by CHIMERE. The soil is represented by relative percentages of sand,  
242 silt, and clay for each model cell. The USGS database, called STATSGO-FAO accounts of 19 different soil types  
243 recorded in the global database with native resolution of  $0.0083 \times 0.0083^\circ$ . To have homogeneous datasets, the  
244 STATSGO-FAO data are re-gridded into the CHIMERE simulation grids. For mineral dust emission calculations,  
245 the land use is typically used to provide a desert mask specifying what surface is potentially erodible.

246

247 The emissions used in this work could still potentially not account for additional misrepresented or unaccounted  
248 sources due to the time difference between the age of the data in the EDGAR and DICE inventories and the  
249 observations used for the validation of the modelling system. The lack of up-to-date national emission inventories  
250 collected at a sufficient resolution, in addition to the lack of research sources providing projections of emissions

251 for 2017, meant that it was not possible to generate more detailed information about the anthropogenic sources of  
 252 emissions for East Africa.



253 **Figure 2:** Annual Totals for the merged emission inventory DICE-EDGAR for year 2017 calculated on the spatial domain at  
 254 18×18 km shown in Figure 1.  
 255

256 It is noted that the time stamp of the anthropogenic emissions and the validation period are different. The emissions  
 257 are relative to year 2013 while the observation used for the validation for 2017. In the absence of additional data  
 258 and in the lack of national or local mitigation policies in the three countries we assume that the differences in time  
 259 stamp do not make large difference to the emission estimates. More detailed analysis of the emission sources and  
 260 the implementation of possible mitigation policies at national and local levels could in future change this situation.

261  
 262 Finally, we recall that one of the main objectives of the present work is to evaluate the performance of WRF and  
 263 CHIMERE models in reproduce meteorology and air pollution levels in urban conurbations using the most-up-to-  
 264 date available data and giving in this way a new insight on the state of the art of the numerical modelling for air  
 265 quality in this area of the world highlighting possible improvements for future works.

266  
 267 **2.4 Weather and Chemistry Observations**

268  
 269 WRF and CHIMERE models have been validated for a limited monthly period between the 14<sup>th</sup> of February and  
 270 14<sup>th</sup> of March 2017. The choice of this period is because of the availability of continuous measurements for the  
 271 validation of both models. While for the case of WRF observations with frequency variable from 3 to 6 hours are  
 272 available from the UK Met Office database for different locations, rarer are PM<sub>2.5</sub> observations that last over one  
 273 month with a measurement frequency of one hour, and from different environments (rural, urban, or roadside  
 274 sites).

276 Moreover, the options chosen for the configuration of the meteorology and chemistry-transport models can result  
 277 in better performance in a season more than in another according to the combination of weather and chemical  
 278 parameters chosen for both models. The February to March time period in East Africa does not have extreme  
 279 temperatures (mean temperatures approximately 10 - 25°C according to the country) and little rainfall that could  
 280 affect the observations of weather conditions and PM<sub>2.5</sub> concentrations (USAID, 2022). These conditions and the  
 281 absence of alternative data covering a large time frame for the validation of CHIMERE have constrained the  
 282 period of simulation to the present period.

283

284 **Table 2:** MIDAS ground weather stations used for the validation of the 2×2 km domains. Station no. corresponds to the  
 285 position of each station in Figure 3a, b and c and PM<sub>2.5</sub> observation points for the urban domains of Addis Ababa, Kampala  
 286 and Nairobi used for the validation of CHIMERE model.

Station n.	Domain	Name	Lat (°)	Lon (°)	Elev. (m)
1	ETH2K	Addis – Bole	0.03	38.75	1900
2		Harar Meda	8.73	38.95	2355
3		Metehara	8.87	39.90	930
		U.S. Embassy (PM <sub>2.5</sub> – urban background)	9.05	38.76	1900
4	UGA2K	Entebbe (Airport)	0.05	32.45	1155
5		Kampala	0.32	32.62	1144
6		Jinja	0.45	33.18	1175
		U.S. Embassy (PM <sub>2.5</sub> – urban background)	0.30	32.59	1150
7	KEN2K	Nairobi (Airport)	-1.32	36.92	1624
8		Embu	-0.50	37.45	1493
9		Nakuru	-0.27	36.10	1901
10		Nyeri	-0.50	36.97	1759
11		Narok	-1.13	35.83	2104
		Tom Mboya Street (PM <sub>2.5</sub> – roadside)	-1.28	36.82	1795
	Nanyuki (PM <sub>2.5</sub> – rural background)	0.01	37.07	1947	

287

288 Observations of temperature, wind speed and directions used for the validation of WRF were taken from the UK  
 289 Met Office MIDAS database (UK, 2012). Data from 11 weather stations, three for the domain of Ethiopia  
 290 (hereafter ETH2K, Figure 3a) and Uganda (hereafter UGA2K, Figure 3b) and five for the domain of Kenya  
 291 (hereafter KEN2K, Figure, 3c) were used to validate the simulations at a resolution of 2×2 km (Table 2).

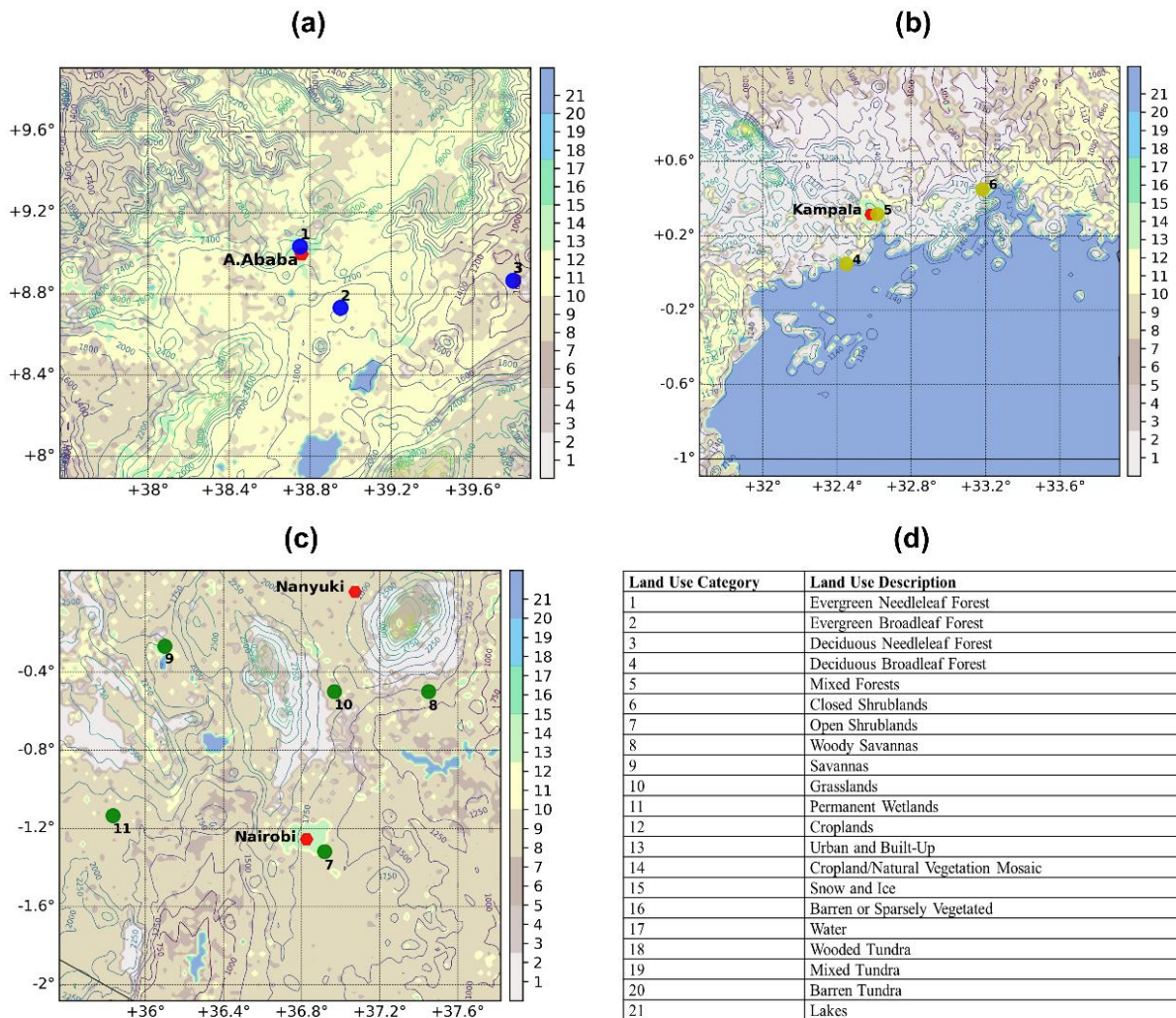
292

293 The ground stations are at different altitudes above sea level to a maximum of 2355 m (e.g., the Harar Meda  
 294 station in Ethiopia, n2 in Figure 3a). The validation was performed by comparing model outputs with observations  
 295 for the variables, namely surface temperature, wind speed and direction and relative humidity. The latter, not  
 296 originally available in the MIDAS dataset, was calculated using the coefficients proposed by Alduchov O. (1996)  
 297 based on hourly surface and dew point temperatures observed values and then compared with modelled data  
 298 obtained by WRF.

299

300 Hourly concentrations of PM<sub>2.5</sub> were used for the validation of CHIMERE for the three internal domains at 2×2  
 301 km (Figure 3a, b, c). For the city of Nairobi, data from roadside background site located at Tom Mboya Street  
 302 was used (1.28° S, 36.82° E), while data from the rural background were provided by a site located in Nanyuki,  
 303 Kenya (0.01° N, 37.07° E). Both the field sites data were obtained from the field sampling campaign performed  
 304 by Pope et al., (2018). For the urban background locations of Addis Ababa and Kampala, hourly concentration of

305  $PM_{2.5}$  were obtained from the air quality monitoring stations of the two U.S. Embassies in Ethiopia (9.05° N,  
 306 38.76° E) and Uganda (0.30° N, 32.59° E) using optical counters. Data from Uganda and Ethiopia were used to  
 307 compare the configuration applied to CHIMERE for Kenya with the two other countries (Table 2).  
 308



309  
 310 **Figure 3:** Second-nested domains at a spatial resolution of 2x2 km centred on the cities of Addis Ababa (ETH2K - a), Kampala  
 311 (UGA2K - b), Nanyuki and Nairobi (KEN2K - c) created using the WRF model outputs. The red dots represent locations of  
 312  $PM_{2.5}$  measurements. The blue, yellow, and green dots refer to the location of the ground weather stations used for the  
 313 meteorological validation in Ethiopia, Uganda, and Kenya, respectively. The numbers relate to the stations detailed in Table  
 314 2. Contour lines are relative to the height meters from the ground levels from WRF outputs while the colour scale applied to  
 315 the maps a, b and c represents the 21 classes of classification of the land use adopted in WRF simulations. The description of  
 316 each land use category is provided in table d.

317

### 318 3 Results and Discussion

319

320 The reliability of numerical simulation of meteorology and chemistry-transport processes need to be evaluated  
 321 against observations from the real world to quantify the confidence of these systems. In the case of CTM in  
 322 particular, this applies also to the capability to be used as tool for policy making, replicating scenarios and analysis  
 323 purposes. While ozone modelling and evaluation has been fairly well developed over a number of decades, with

324 the EPA (1991) criteria still used to evaluate the level of confidence of a CTM, for the PM evaluation the criteria  
325 used for the analysis of the performance are still evolving (Boylan and Russell, 2006).

326

327 In this work we use different statistical operators to evaluate the performance of WRF and CHIMERE models in  
328 reproducing the main surface weather parameters and hourly and daily concentrations of PM<sub>2.5</sub> in different urban  
329 and rural environments. The statistical parameters of Pearson's Coefficient (R), index of agreement (IOA), mean  
330 fractional bias (MFB) and mean fractional error (MFE) have been used for the calculations.

331

332 MFB and MFE in particular, are metrics specifically used for the evaluation of numerical system for atmospheric  
333 chemistry and meteorology. They normalise the bias and the error for each model-observed pair by the average  
334 of the model and observation before taking the final average (Eq. 2 and 3). The advantage of these metrics is that  
335 the maximum bias and errors are bounded, and that impact of outlier data points are minimised. Moreover, the  
336 metrics are symmetric giving equal weight, to concentrations simulated higher than observations and to those that  
337 are simulated lower than observations.

338 
$$MFB = \frac{1}{N} \sum_{i=1}^N (C_m - C_o) / ((C_o + C_m) / 2) \quad \text{Eq. (2)}$$

339

340 
$$MFE = \frac{1}{N} \sum_{i=1}^N |C_m - C_o| / ((C_o + C_m) / 2) \quad \text{Eq. (3)}$$

341

342 MFB and MFE have been expressed in terms of model performance "goals" and model performance "criteria"  
343 values according to the methodology proposed by Boylan and Russell (2006). The performance "goal" for the  
344 modelling system is attested for  $MFE \leq 50\%$  and  $MFB \leq \pm 30\%$ . In this range of values (shown as green dashed  
345 lines in Figure 6) the performance of the model in reproducing the correct magnitude of the concentrations can be  
346 considered good. A second larger range of values, called "criteria", is attributed for  $MFE \leq 75\%$  and  $MFB \leq \pm$   
347  $60\%$ . Values inside this are (shown as red dashed lines in Figure 6) corresponds to an average model performance.  
348 Finally, values with  $MFE > 75\%$  and  $-60\% > MFB > +60\%$  correspond to a poor representation by the model  
349 (labelled "out" in Table 5).

350

351 WRF and CHIMERE models run at spatial resolutions of 18×18, 6×6 and 2×2 km for meteorology and at 6×6 and  
352 2×2 km for chemistry for the three domains of East Africa. The statistical analysis shown in the following sections  
353 though, describes the validation results for the three internal domains at a resolution of 2×2 km as these are the  
354 focus of the present work.

355

356 Ground weather stations from the MIDAS database, included in the 2×2 km domains of all countries, were  
357 analysed individually, and shown as average of all stations. The time series and wind roses are relative to the  
358 closest stations from MIDAS database to each urban city centre of the three capital cities, namely Addis- Bole  
359 (n1 in Table 2), Kampala (n5 in Table 2) and Nairobi Airport (n7 in Table 2).

360

361 Initially, the performance of CHIMERE was analysed for the domain of Kenya for which hourly concentrations  
362 of PM<sub>2.5</sub> were taken from two different sites (roadside and rural) from the field sampling campaign described by  
363 Pope et al., (2018). Secondly, the same configuration adopted for Kenya was used for Ethiopia and Uganda to test

364 both the homogeneity of the emission rates on other urban conditions, and the configuration chosen for CHIMERE  
365 in different urban and environmental conditions. At this stage of the validation, a threshold limit of  $25 \mu\text{g m}^{-3}$  for  
366  $\text{PM}_{2.5}$  per day provided by WHO (WHO, 2005) was used to quantify the number of exceedances observed and  
367 modelled by CHIMERE for the three cities.

368  
369 The validation process was hindered by the highly variable quantity and quality of available meteorological data.  
370 The majority of the weather observations are provided on a 3-hourly basis, with varying amounts of missing data.  
371 Despite this, the statistical evaluation of WRF has been performed comparing model and observations only when  
372 the latter were available. We recall that the objective of this work aims to test the performances of a modelling  
373 system for the simulation of air quality at high resolution for East Africa, updating and/or using the available input  
374 data available and assessing the possible adoption of these tools for air quality policy making at this extent of the  
375 data.

376

### 377 **3.1 Validation of the WRF simulations**

378

379 In order to assess the performance of WRF in simulating surface temperature, relative humidity wind speed and  
380 direction, the model simulation outputs were compared with all the available ground weather station data available  
381 for the period of analysis, 14<sup>th</sup> of February to 14<sup>th</sup> of March 2017. Observations from the UK Met Office MIDAS  
382 database were available with variable frequency ranging from 1 to 6 hours.

383

#### 384 *3.1.1 Statistical evaluation of WRF performances*

385

386 A statistical analysis, in terms of the mean fractional bias (MFB), mean fractional error (MFE), index of agreement  
387 (IOA) and Pearson's coefficient (R), was carried out to compare modelled and observed values for the domain at  
388  $2 \times 2$  km resolution averaging the observed and modelled values on all the stations present on each domain (Table  
389 3). We recall that the number and location of the stations is variable between the three domains (3 stations for  
390 ETH2K and UGA2K and 5 stations for KEN2K).

391

392 The results of the statistical analysis show that WRF is capable of reproducing the mean levels of surface  
393 temperature better for the domain of Ethiopia (ETH2K) and Uganda (UGA2K) with a mean underestimation over  
394 the three domains of 1.4 and 1.5 °C, respectively, then for Kenya (KEN2K) where it shows an underestimation of  
395 4.1 °C. The higher bias in surface temperature found on the average of all five stations of Kenya is though highly  
396 driven by a particular poor representation of this variable at the observation point of Narok (n11 in Figure 3c)  
397 where the bias between model and observations is 10.9 °C. A reason for this bias can be related by the location of  
398 the station that is the one at highest altitude of all the Kenyan weather stations (2104 m a.g.l.). Narok is located  
399 around 140 km west from Nairobi and the high bias in temperature should not have any effect on the levels of  
400 temperature modelled in the capital of Kenya were the bias for the individual station of Nairobi (n7 in Figure 3c)  
401 found was 1.3 °C.

402

403 Relative humidity is overestimated by WRF in KEN2K of 0.2 % and underestimated in ETH2K of 6.4 % and in  
 404 UGA2K of 7.5 % (Table 3). Wind Speed and directions for the three domains show respectively, the presence of  
 405 northern winds in UGA2K correctly captured by the model with a difference of around 4 degrees in comparison  
 406 with the observations, an average eastern wind component in KEN2K partially reproduced by the model that  
 407 allocates the average wind directions on a more south-eastern component of wind with a difference of around 40.2  
 408 degrees while in ETH2K the average wind direction modelled and observed are closer with a difference of 4.2  
 409 degrees on a south-eastern component of prevailing wind. The observed and modelled wind speeds in UGA2K,  
 410 KEN2K and ETH2K are in reasonable agreement with a model overestimation of 0.9, 0.8 and 0.2 m s<sup>-1</sup>,  
 411 respectively (Table 3).

412

413 **Table 3:** Statistical analysis of relative humidity, surface temperature, wind speed and directions averaged on all the available  
 414 weather stations for the second nested domains UGA2K, KEN2K and ETH2K at 2×2 km of resolution. Mean observed and  
 415 modelled values (Obs. Mean, Model Mean), Pearson's Coefficient (R), index of agreement (IOA), mean fractional bias (MFB)  
 416 and error (MFE) have been calculated.

	Rel. Humidity (%)			Temperature (°C)		
	UGA2K	KEN2K	ETH2K	UGA2K	KEN2K	ETH2K
<b>Obs. Mean</b>	68.2	63.1	51.3	24.5	23.2	22.7
<b>Model Mean</b>	60.7	63.3	44.9	23.0	19.1	21.3
<b>MFB</b>	-21.52	-21.36	-33.02	0.17	-24.25	-5.38
<b>MFE</b>	30.08	32.25	35.56	12.50	27.94	11.34
<b>IOA</b>	0.44	0.44	0.47	0.43	0.31	0.53
<b>R</b>	0.3	0.4	0.7	0.3	0.5	0.6
	Wind Dir (degrees)			Wind Speed (m s <sup>-1</sup> )		
	UGA2K	KEN2K	ETH2K	UGA2K	KEN2K	ETH2K
<b>Obs. Mean</b>	6.8	91.5	104.0	2.5	2.7	3.5
<b>Model Mean</b>	2.8	131.7	99.8	3.4	3.5	3.7
<b>MFB</b>	32.02	-30.57	-9.94	91.25	36.83	18.89
<b>MFE</b>	62.01	70.55	60.18	94.59	54.35	50.63
<b>IOA</b>	0.39	0.40	0.46	0.26	0.41	0.31
<b>R</b>	0.3	0.2	0.2	0.1	0.5	0.4

417

418 All the relative humidity and surface temperature values of MFE were found in the performance goal range for  
 419 the three domains: UGA2UK (30.08 and 12.50, respectively) KEN2K (32.25 and 27.94) and ETH2K (35.56 and  
 420 11.34). The same evaluation done on wind direction and speed shows for the former MFE values inside the criteria  
 421 performance range (62.01 for UGA2K, 70.55 for KEN2K and 60.18 for ETH2K) but for wind speed only KEN2K  
 422 and ETH2K are in the criteria range (54.35 and 50.63, respectively) while wind speed in UGA2K is found outside  
 423 the range of acceptability of the metric (94.59) (Table 3). The MFB analysis shows that surface temperature is  
 424 inside the range of performance goal in all three domains with UGA2K (0.17) showing the best performance in  
 425 reproducing the variable followed by ETH2K (-5.38) and KEN2K (-24.25). The MFB values inside the goal  
 426 criteria were found for the domain of UGA2K and KEN2K also for relative humidity (-21.52 and -21.36) while  
 427 for ETH2K the value of MFB was found in the criteria range (-33.02). The ETH2K is the only domain that shows  
 428 MFB in the goal range for the evaluation of wind direction (-9.94) and speed (18.89). The domain of Kenya  
 429 (KEN2K) shows both values inside the criteria range with -30.57 for wind direction and 36.83 for wind speed.

430 Finally, UGA2K shows wind direction inside the criteria range (32.02) but wind speed outside the range of  
431 acceptability of this metric (91.25) (Table 3).

432

433 The calculated Pearson's coefficient (R) shows varying agreement between the model and observations with  
434 values between 0.1 and 0.7 for the three domains. The highest R value for relative humidity of approximately 0.7  
435 was obtained for ETH2K while the lowest R values occurred in UGA2K (0.3). The highest value of R for surface  
436 temperature was found in ETH2K (0.6), followed by KEN2K (0.5) and UGA2K (0.3). For wind speed, the highest  
437 R coefficient value is for KEN2K (0.5) and the lowest for UGA2K (0.1) while for wind directions, the highest R  
438 value found was for UGA2K (0.3) with values of approximately 0.2 for the other two domains (Table 3).

439

440 Finally, the evaluation of the index of agreement (IOA) shows values for surface temperature between 0.31  
441 (KEN2K) and 0.53 (ETH2K) and values between 0.44 and 0.47 for relative humidity in the three domains. For  
442 wind speed and directions, the IOA varies between 0.39 (UGA2K) and 0.46 (ETH2K) for the former and between  
443 0.26 (UGA2K) and 0.41 (KEN2K) for the latter.

444

#### 445 *3.1.2 Hourly variation of Temperature and Relative humidity*

446

447 The three MIDAS stations providing weather observations closest to the urban areas of the Addis Ababa, Kampala  
448 and Nairobi have been analysed individually in form of hourly time series of surface temperature and relative  
449 humidity and wind roses for wind speed and directions.

450

451 The hourly surface temperature and relative humidity are shown in Figure 4 for the three ground weather stations  
452 closest to the centre of the three cities: Addis Bole (n1 in Figure 3a), Kampala Station (n5 in Figure 3b) and  
453 Nairobi (n7 in Figure 3c).

454

455 The temperature range observed at the three stations was between 9 and 27° C for the Addis Bole Station, 16 and  
456 31° C for Kampala and 16 and 33° C for Nairobi. By inspection of Figure 4, it can be seen that the WRF model  
457 is able to reproduce the main diurnal cycle of variation of temperature and relative humidity for the three ground  
458 weather stations. Surface temperature peaks are slightly underestimated by the model for the three stations with a  
459 small mean bias at the three stations between -0.06 and -0.1° C. The highest agreement between the model and  
460 observation is for Kampala while the model tends to underestimate the diurnal peaks of surface temperature almost  
461 systematically for Addis Bole and Nairobi stations.

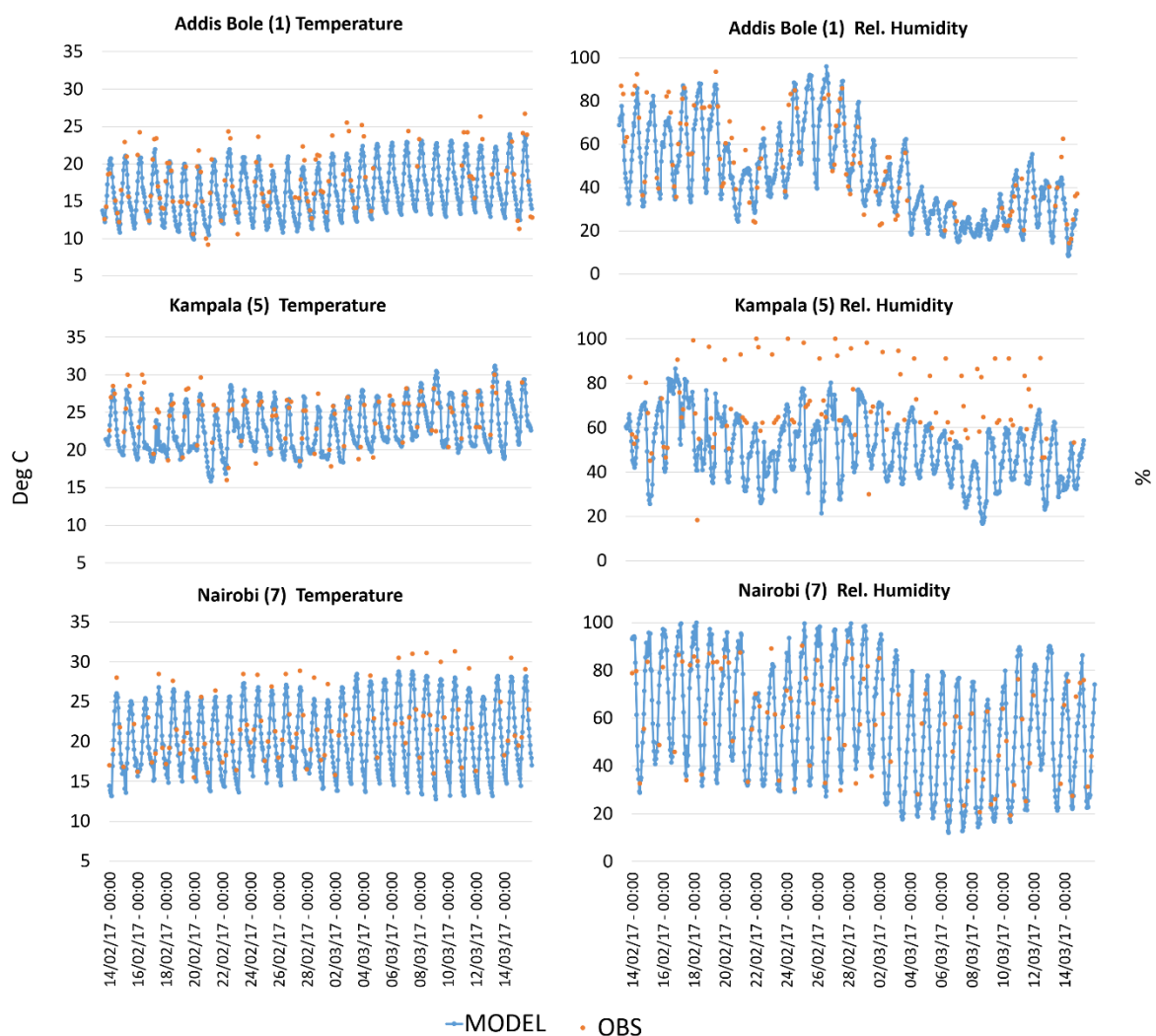
462

463 The mean relative humidity observed at the three stations shows different ranges of excursion from the model  
464 predictions depending on the characteristics of the environment. The station of Addis Bole shows the higher  
465 variation from 15 to 98 %, Nairobi station from 17 to 98 % and Kampala from 19 to 99 %. From Figure 4, it may  
466 be seen that relative humidity variations over time are correctly captured by WRF for the Nairobi and Addis Bole  
467 stations. Despite this both the diurnal peaks and night lowest values seems to be not correctly reproduced by the  
468 model that tends to overestimate the formers and underestimate the latter with a bias between -0.1 and 0.004 %.

469

470 However, WRF appears systematically to underestimate the relative humidity for the Kampala station showing a  
 471 mean negative bias. Different reasons could affect the underestimation of the relative humidity at this station. The  
 472 sensitivity of WRF model to the land use data (Teklay et al., 2019) connected with the proximity of Kampala to  
 473 Lake Victoria, which is a massive inland body of water (surface area 68,800 km<sup>2</sup>) could influence the local  
 474 variation of relative humidity in ways which are not well reproduced by the model. The influence of Lake Victoria  
 475 and of the Kampala's complex topography on measurements of relative humidity was previously highlighted by  
 476 Singh et al. (2020) in relation to monthly visibility connected with PM levels. It has to be noted that relative  
 477 humidity was calculated from surface temperature and dew point values following Alduchov O. (1996) and not  
 478 directly sampled. A better agreement in the simulation of relative humidity from WRF can be found in the station  
 479 of Entebbe (n4 in Figure 3b) where the mean normalized bias shows a small underestimation of 0.04 %.

480

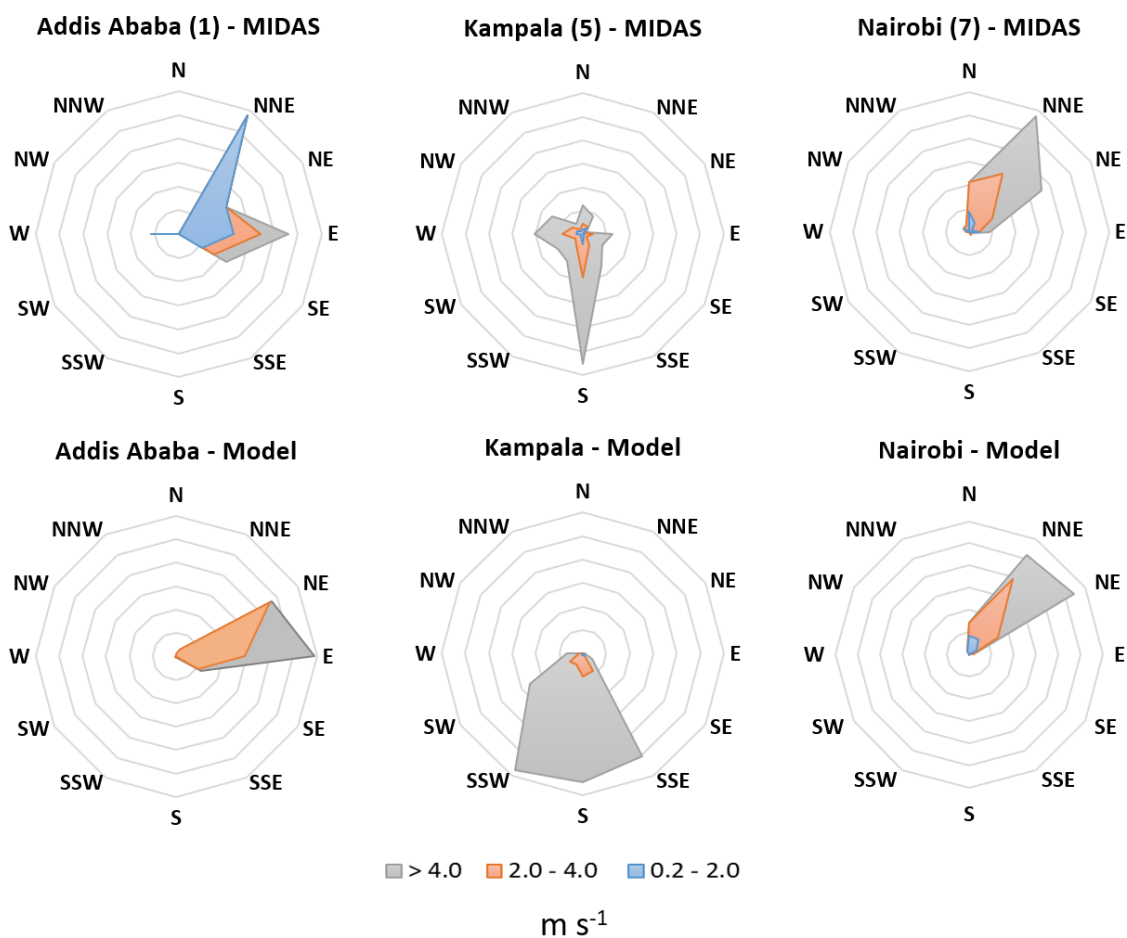


481 **Figure 4:** Hourly time series of surface temperature (left column) and relative humidity (right column) for the closest ground  
 482 weather stations to the urban centres of the cities of Addis Ababa (station 1 in Figure 3a), Kampala (station 5 in Figure 3b)  
 483 and Nairobi (station 7 in Figure 3c). Comparison between modelled values (blue lines) obtained from the 2×2 km domains  
 484 and hourly observations (orange spots) from MIDAS database.

485

486

487 Wind speed and directions from the urban stations of Addis Bole (n1 in Figure 3a), Kampala Station (n5 in Figure  
 488 3b) and Nairobi (n7 in Figure 3c) are shown in Figure 5 in the form of wind roses. WRF can reproduce the average  
 489 wind directions in close agreement with the observed data for the analysed period for Nairobi showing the  
 490 predominance presence of North-North-Eastern winds with high speed ( $> 4.0 \text{ m s}^{-1}$ ). Wind speed observations  
 491 from the ground weather station of Kampala also suggest a strong southern wind component ( $> 4.0 \text{ m s}^{-1}$ ) while  
 492 the model seems to reproduce a similar magnitude of the wind speed but on a larger range of directions ranging  
 493 from the South-South-East direction to South-South-West. For Addis Ababa, WRF seems able to capture and  
 494 reproduce the main wind directions observed for the simulated period, e.g., Eastern and North-Eastern winds.  
 495 Despite this, slower winds between  $0.2$  and  $2.0 \text{ m s}^{-1}$  with a strong North-Northeast component do not seem to be  
 496 replicated by the model for the station located inside the capital of Ethiopia.



497  
 498 **Figure 5:** Averaged wind roses for the whole analysed period (14<sup>th</sup> of February to 14<sup>th</sup> of March 2017) from the closest ground  
 499 weather stations to the urban centres of Nairobi (n7 in Figure 3c), Kampala (n5 in Figure 3b) and Addis Ababa (n1 in Figure  
 500 3a) (MIDAS, top) and from WRF simulation outputs (Model, bottom).

501  
 502 The lower agreement in the reproduction of the wind speed and direction in Addis Bole and Kampala stations can  
 503 be connected to the particular locations of both stations. The difference in the location of the observations can, in  
 504 fact, influence rapid changes in directions and speed locally recorded and not reproduced by the model. In the  
 505 case of Kampala, the airport is located near the coast of the Lake Victoria where the local conditions of wind are

506 more susceptible of variation and can be erroneously reproduced by the model. In the case of Addis Bole, the only  
507 station settled in the urban area, the urban topography and possible canyon effects of the wind can be not well  
508 captured by the model that reproduces a more constant range of wind speed and directions not accounting for  
509 quick variations at low speed observed at the station.

510

511 The results obtained from the validation of the meteorological simulations performed over East African domains  
512 using WRF show that the model is on average able to reproduce all four variables taken in account close to the  
513 observed data in the 2×2 km domains with variable agreement between the three cities. The highest agreement in  
514 the weather analysis has been found for surface temperature with similar biases to Kerandi et al. (2017) and  
515 relative humidity similar to Pohl et al. (2011), which is sufficiently accurate to be able to use these values for the  
516 physical calculations done by the chemistry transport model.

517

518 Nevertheless, the more detailed analysis of the urban weather stations revealed discrepancies in the reproduction  
519 of relative humidity and wind direction for the station of Kampala (UGA2K) that could affect the deposition,  
520 removal and transport processes simulated by CHIMERE and will be object of future investigation to further  
521 improve the meteorological performance of WRF. However, for the purposes of the present work the range of  
522 bias found for the meteorological variables can be considered acceptable. Even if the bias found for some variable  
523 in the calculation of the averaged statistics over all stations was high, the individual weather stations close to the  
524 urban areas of interest showed smaller bias and levels of MFB and MFE inside the goal or criteria range of  
525 performance and therefore considered acceptable for simulations.

526

### 527 **3.2 Validation of CHIMERE simulations**

528

529 The CHIMERE validation has been focused on the hourly levels of PM<sub>2.5</sub> modelled at the two observation sites  
530 for the domain KEN2K, representative of a roadside site and a rural background site. Also, from the urban  
531 background observational sites of the U.S. Embassies of Kampala (UGA2K) and Addis Ababa (ETH2K). The  
532 performance of CHIMERE was analysed also in terms of mean fractional error (MFE), mean fractional bias  
533 (MFB) and Pearson's coefficient (R) against the different level of average concentrations of PM<sub>2.5</sub> in the four  
534 observation points to evaluate the response of the model in reproducing low and high levels of hourly  
535 concentrations in comparison with observed values.

536

537 The validation of CHIMERE was done for the domains at highest resolution (2×2 km) despite the availability of  
538 emissions at a similar spatial resolution. The reason of this choice is motivated by the necessity to validate the  
539 reliability of the model against observation data from particular locations in different backgrounds. In order to  
540 better configure the model to represent the different urban and rural environments it is necessary to take in account  
541 the uncertainties of a model representation against an observation point. One cause of uncertainty when comparing  
542 modelling outputs with observations is the difference between a point measurement and a volumetric grid cell  
543 averaged modelled concentration (Seinfeld, 2016). On one hand, the extent of a measurement point, in fact,  
544 represents only the extent of the nearby points or an average concentration in a specified area. On the other hand,

545 a surface level modelling grid typically has highest resolution of 1 km with a vertical height of between 20 and  
546 40 m and the concentration represented by the model is the average over the entire grid cell.

547

548 In the particular case of the domains of East Africa, CHIMERE simulates at coarse resolution e.g., the 6×6 km,  
549 values of concentration representative of an average of 36 km<sup>2</sup>, difficult to be compared with observations taken  
550 in a particular point. Increasing the spatial resolution and bringing it to 2×2 km the average value inside each grid  
551 cell will be representative of a smaller area such as 4 km<sup>2</sup> whose average value can be closer compared with an  
552 individual observation point.

553

### 554 *3.2.1 Statistical evaluation of model performances*

555

556 The absolute bias between mean observed and modelled concentrations of PM<sub>2.5</sub> shows an overestimation of the  
557 model for the domain KEN2K by between 0.01 and 3.7 µg m<sup>-3</sup> for Nanyuki and Nairobi, respectively, and for  
558 Addis Ababa (0.6 µg m<sup>-3</sup>). On the contrary, the model underestimates PM<sub>2.5</sub> for the domain UGA2K (Kampala)  
559 by 7.2 µg m<sup>-3</sup> (Table 4).

560

561 The mean fractional bias (MFB) and error (MFE) for the two Kenyan observation points were found in both cases  
562 inside the goal performance criteria with MFE ≤ 50% and MFB ≤ ± 30% both in Nairobi (roadside site) and in  
563 Nanyuki (rural site). The hourly MFB and MFE were 4.88 and 25.39 for Nairobi and 3.36 and 8.33 for Nanyuki  
564 while 0.1 and 1.99 for Nairobi and 1.08 and 4.73 for Nanyuki were the respective values found for the daily  
565 analysis.

566

567 The MFB and MFE analysis for the urban background site in Addis Ababa showed values inside the range of the  
568 goal criteria both for the hourly (2.93 and 29.99 for MFB and MFE) and for daily analysis (8.23 and 2.86). Finally,  
569 in the urban background site of Kampala the MFB were found inside the goal criteria both for daily (-11.28) and  
570 hourly (-7.60) analysis, while for the MFE the hourly analysis showed a value in the range of the criteria range  
571 (32.99) but daily MFE in the goal performance range (22.06) (Table 4).

572

573 The highest Pearson's coefficients (R) were found in Nanyuki with hourly and daily values of between 0.91 and  
574 0.93. The roadside site of Tom Mboya Street in Nairobi had R values of between 0.35 and 0.38 while the urban  
575 background sites of Addis Ababa and Kampala had a lower agreement an hourly level (R values were between  
576 0.10 and 0.29, respectively) than at a daily level (R values of between 0.42 and 0.30, respectively).

577

578 In general, the statistical analysis demonstrates that the model can reproduce the daily pattern of the hourly  
579 changes in concentrations for the two pollutants both in the three urban/roadside sites and in the rural site  
580 considered. The low R coefficient values obtained for the urban domains at the hourly level suggests that sources  
581 of anthropogenic emissions affecting urban air quality are still missing from the current emission inventory.  
582 Further work will be focused on the improvement of the magnitude of the emissions to better match the observed  
583 levels of concentrations of particulate matter at the urban level. Despite this and considering the daily average

584 concentrations in the urban sites, the R coefficients were found to be between 30 and 42 % suggesting that  
 585 CHIMERE better reproduces the concentrations of PM<sub>2.5</sub> using daily averaging.

586

587 The performance of CHIMERE varies between the domains of Kenya, Uganda, and Ethiopia. The performance  
 588 of the model has been optimised during the validation for the simulation of hourly concentrations of PM<sub>2.5</sub> in  
 589 Kenya and the same configuration applied to the domain of Uganda and Ethiopia to compare the reliability of the  
 590 model. The difference in performance can be connected to different reasons: In first place, the difference in the  
 591 sampling methods used for the two sites in Kenya against the measurements taken in the U.S. Embassies of  
 592 Kampala and Addis Ababa. Secondly, another element of differentiation can be connected to the location of the  
 593 observation sites in the cases of the U.S. Embassies and/or the possible influence of local sources not accounted  
 594 in the emission inventories.

595

596 **Table 4:** Hourly and daily statistical evaluation of CHIMERE model performance for the cities of Nairobi against ASAP  
 597 observed data and against U.S. Embassies data for the cities of Addis Ababa and Kampala.

ASAP OBS	NAIROBI PM <sub>2.5</sub> (µg/m <sup>3</sup> ) roadside		NANYUKI PM <sub>2.5</sub> (µg/m <sup>3</sup> ) rural	
	DAILY	HOURLY	DAILY	HOURLY
Mean MOD	58.3	58.3	3.24	3.24
Mean OBS	54.6	54.6	3.23	3.23
MFB	0.1	4.88	1.08	3.36
MFE	1.99	25.39	4.73	8.33
R	0.38	0.35	0.93	0.91
U.S. EMBASSY OBS	ADDIS A. – PM <sub>2.5</sub> (µg/m <sup>3</sup> ) urban		KAMPALA – PM <sub>2.5</sub> (µg/m <sup>3</sup> ) urban	
	DAILY	HOURLY	DAILY	HOURLY
Mean MOD	18.7	18.7	36.2	36.2
Mean OBS	18.1	18.1	43.4	43.4
MFB	8.23	2.93	-11.28	-7.60
MFE	2.86	29.99	22.06	32.99
R	0.42	0.10	0.30	0.29

598

599

600 Finally, the site of Nanyuki is the location where the agreement between model and observations is highest. This  
 601 site was chosen by Pope et al. (2018) as rural spot in a location of minimum local air pollution useful to calculate  
 602 the net urban increment subtracting the rural background concentrations of Nanyuki from the urban concentrations  
 603 in Nairobi. Is therefore intended by their work that the average concentrations in that site were really low. The  
 604 model is able to reproduce this low level of contamination close to the reality and to reproduce also peaks of  
 605 contamination in particular days of February probably generated elsewhere (see Section 3.2.2).

606

607 The MFB and MFE analysis have been conducted also at hourly level comparing modelling outputs and  
 608 observations from all six sites in relation to the magnitude of hourly concentrations (Figure 6).

609

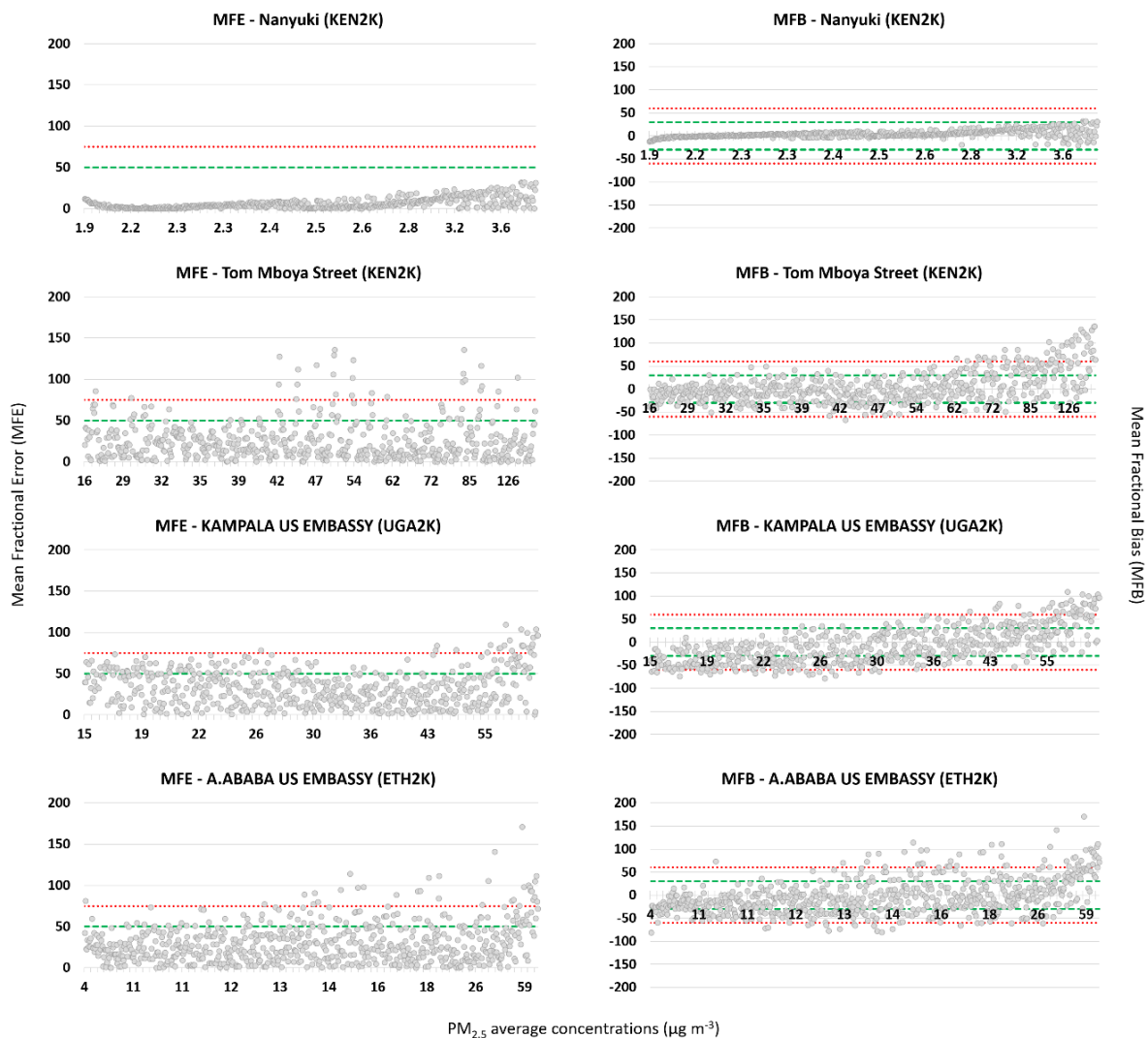
610 There are some MFB values outside the criteria range for PM<sub>2.5</sub> for the urban sites of Addis Ababa and Kampala  
 611 and for the roadside site of Tom Mboya Street in Nairobi. In terms of the upper limit (MFB > 60 %) these values  
 612 tend to be concentrated between 60 and 130 µg m<sup>-3</sup> for Tom Mboya Street, 40 and 55 µg m<sup>-3</sup> for Kampala and

613 between 13 and 59  $\mu\text{g m}^{-3}$  for Addis Ababa (Figure 6). A much smaller number of MFB values for the Addis  
 614 Ababa and Kampala sites are less than the lower criteria limit and these tend to be for lower concentrations  
 615 between 10 and 26  $\mu\text{g m}^{-3}$ .

616

617 MFE values outside the ranges of criteria are between 42-55 and 80-130  $\mu\text{g m}^{-3}$  for Tom Mboya Street, 43 and 60  
 618  $\mu\text{g m}^{-3}$  for Kampala and 13 and 59  $\mu\text{g m}^{-3}$  for Addis Ababa (Figure 6). The latter two sites present a more variability  
 619 of MFB and MFE in comparison with the two sites of Kenya where is visible a common positive bias of the model  
 620 in reproducing the highest concentration levels. The reliability of the model is therefore higher for the domain of  
 621 Kenya, both for a rural and for a roadside site than for the two urban background sites in Uganda and Ethiopia.

622



623

624 **Figure 6:** Hourly mean fractional bias (MFB) and mean fractional error (MFE) values calculated for the locations of Tom  
 625 Mboya Street and Nanyuki (KEN2K), Kampala U.S. Embassy (UGA2K) and Addis Ababa U.S. Embassy (ETH2K) for the  
 626 analysed period against hourly concentrations of PM<sub>2.5</sub>. The green lines represent the MFB range  $\pm 30\%$  and the MFE limit  
 627 of 50% for which the model performance can be considered reliable, the red lines represent the MFB range  $\pm 60\%$  and the MFE  
 628 limit of 75% for which model performance can be increased by diagnostic analysis on the chemical precursors of PM<sub>2.5</sub>.  
 629

630 The overall performance of the model against different levels of concentrations is summarised in Table 5. The  
 631 PM<sub>2.5</sub> reproduced at the two sites in KEN2K shows a higher percentage of values within the MFB and MFE

632 performance goals for the rural site of Nanyuki, than for Tom Mboya Street. e.g., 97 % compared to 69 % and 99  
 633 % compared to 88 % for the MFB and MFE measures respectively. For the criteria measure, the corresponding  
 634 percentages are 2 % vs. 22 % and 1 vs. 7 % (Table 5).

635  
 636 The percentages for the urban sites of Kampala and Addis Ababa show a lower agreement between the model and  
 637 observations. For the former 48 % of the values according to the MFB measure are within the goal range, 37 %  
 638 are within the criteria range and 15 % are outside. For the latter, according to the MFB criteria, 57 % of the values  
 639 are inside the goal range, 30 % of values are within the criteria range and 13 % are outside. In terms of the MFE  
 640 measure, 74 % and 80 % of values for the two cities are within the goal range, 16 % and 11 % within the criteria  
 641 range and 10 % and 9 % outside respectively (Table 5).

642  
 643 **Table 5:** Hourly mean fractional bias (MFB) and error (MFE) percentage of points inside the goal limit (GOAL), inside the  
 644 diagnostic range (CRITERIA) and outside the reliability criteria (OUT) from model outputs extracted from the four analysed  
 645 locations.

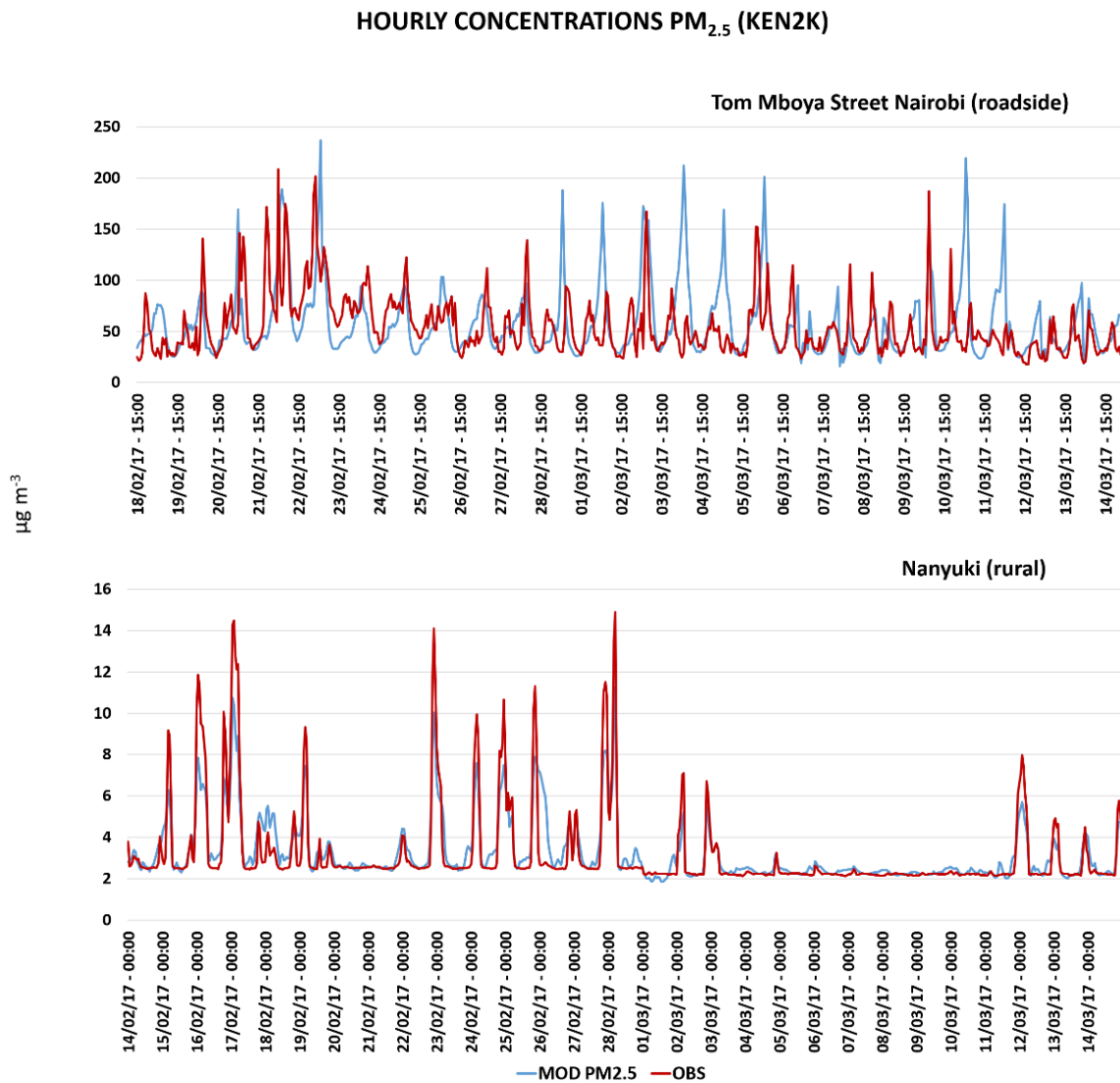
City	MFB			MFE		
	GOAL (%)	CRITERIA (%)	OUT (%)	GOAL (%)	CRITERIA (%)	OUT (%)
<b>Tom Mboya St. (KEN2K)</b>	69	22	9	88	7	5
<b>Nanyuki (KEN2K)</b>	97	2	1	99	1	0
<b>Kampala (UGA2K)</b>	48	37	15	74	16	10
<b>A. Ababa (ETH2K)</b>	57	30	13	80	11	9

646  
 647 According to the methodology proposed by (Boylan and Russel, 2006) the performance of a modelling system is  
 648 fairly good for PM<sub>2.5</sub> representation if about the 50 % of the points are within the goal range and a large majority  
 649 are within the criteria range. From the analysis of the four sampling sites the values of MFB inside both the goal  
 650 and range for Tom Mboya Street are 69 %, 97 % for Nanyuki and 57 % for Addis Ababa and only for Kampala  
 651 are 48 %. Similarly, for the MFE measure, 99 % for Nanyuki, 88 % for Tom Mboya Street, 80 % for Addis Ababa  
 652 and 74 % for Kampala are inside both the goal range. The demonstrates that the performance of the model can be  
 653 considered to be satisfactory (Table 5).

654  
 655 Finally, the reason for the presence in the Addis Ababa and Kampala simulations of values outside the criteria  
 656 range both at high and at low concentrations of PM<sub>2.5</sub> can be connected to the representation of the original PM  
 657 emissions in the combined inventory. It is possible that CHIMERE is not able to correctly reproduce all the  
 658 chemical processes involved in the secondary formation of inorganic and organic individual components of PM<sub>2.5</sub>  
 659 with the extent of the present input data. Moreover, the possible misrepresentation of local emission sources not  
 660 reproduced in DICE-EDGAR can also affect the performance of the model. Finally, the different location of the  
 661 urban background observation sites and the sampling techniques for PM observation can also have a key role in  
 662 the correct detection of the concentrations.

663  
 664 *3.2.3 Hourly variation of PM<sub>2.5</sub> in urban and rural sites of Kenya*  
 665

666 Hourly modelled variation of PM<sub>2.5</sub> levels obtained by CHIMERE compared with observations are shown for the  
 667 urban sampling site of Tom Mboya Street in Nairobi and for the rural site of Nanyuki (Figure 3c).  
 668



669  
 670 **Figure 7:** Hourly time series for PM<sub>2.5</sub> from the roadside of Tom Mboya Street (top) and from the rural site of Nanyuki (bottom)  
 671 from modelled output from CHIMERE model (blue line) and observed values from Pope et al. (2018) (red line) for the analysed  
 672 period. The simulation started on the 14<sup>th</sup> of February. For the Tom Mboya Street site only the period of time between the 18<sup>th</sup>  
 673 of February and the 14<sup>th</sup> of March when observations were available has been shown in the timeseries.  
 674

675 By inspection of Figure 7 it can be seen that CHIMERE is able, in general, to reproduce the daily variation of  
 676 PM<sub>2.5</sub> across the simulated period at both sites. The magnitude of the emissions adopted seems to be suitable both  
 677 for the roadside area of Tom Mboya Street and for the rural background site of Nanyuki, with higher agreement  
 678 shown by the latter. CHIMERE captures only part of the daily peak observed in Tom Mboya Street with  
 679 comparable magnitude but misrepresents some peaks. In particular it models higher hourly peaks than those  
 680 observed as previously mentioned in the MFB and MFE analysis.  
 681

682 The misrepresentation of some high peaks in Tom Mboya Street is possibly due to a number of different reasons.  
683 Firstly, is important to recall that the point measurements and relative observed concentrations are representative  
684 of a smaller portion of space in comparison with grid-cell concentrations modelled. In this particular case the  
685 comparison is between a roadside site subjected to possible additional local sources of PM<sub>2.5</sub> not accounted for in  
686 the emissions and not correctly reproduced by CHIMERE. On the other hand, a few of the modelled peaks were  
687 overestimated. This can be addressed by improved temporal description of the emissions and in their magnitude  
688 in comparison to the reality. As mentioned previously, the anthropogenic emissions used in this work were the  
689 most up-to-date available at the time and that there is inevitably some difference between the measured data due  
690 to the difference in time between the inventories and the measurements. Despite this, there is reasonable agreement  
691 between model outputs and observed concentrations for the majority of the analysed period highlighting the  
692 reliability of CHIMERE in describing the hourly concentrations trends for a roadside site with expected high  
693 levels of PM<sub>2.5</sub> contamination.

694  
695 Similarly, in the rural site of Nanyuki, the model seems to correctly reproduce the hourly variation of the  
696 concentrations during the whole period, underestimating the maximum peaks at the beginning of February and in  
697 the last four days of simulation in March. (Figure 7). The site shows different magnitude in the concentrations of  
698 PM<sub>2.5</sub> when comparing the February and March periods. While between the 4<sup>th</sup> and the 10<sup>th</sup> of March hourly  
699 concentrations are around 3-4 µg m<sup>-3</sup>, previously and subsequently to this period of time, the concentrations of  
700 PM<sub>2.5</sub> are more than two times higher. This behaviour is visible both in the observations from the site (red line in  
701 Figure 7, bottom) and from the model outputs obtained using CHIMERE (blue line in Figure 7, bottom).

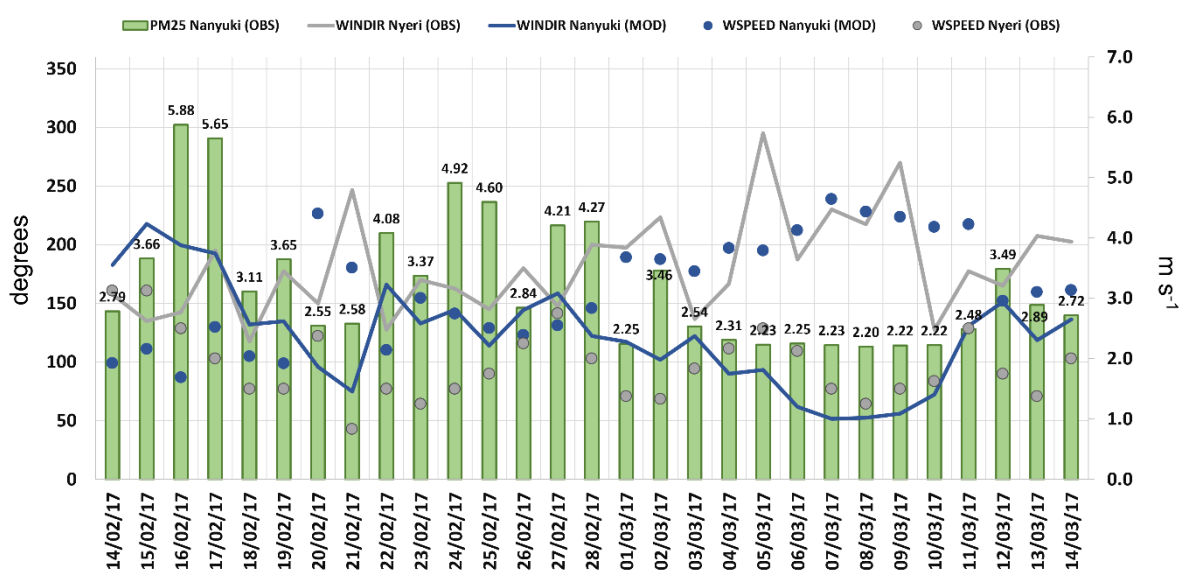
702  
703 One of the few possible reasons for this different behaviour may be connected to dispersion of pollutants in  
704 particular weather conditions of wind speed and wind directions during February and March in the area. To  
705 investigate this possible explanation, we consider the closest MIDAS weather station to the sampling area of  
706 Nanyuki, in the town of Nyeri (0.43° S, 36.95° E altitude 1916 m a.g.l.) (n10 in Figure 3). Nyeri is only 60 km  
707 from the Nanyuki site and is situated between Mount Kenya (0.10° S, 37.30° E, altitude 4341 m a.g.l.) to the west  
708 and the Aberdare Range (0.46° S, 36.69° E, altitude 3441 m a.g.l.).

709  
710 The daily average concentrations observed in the sampling site of Nanyuki have been compared with the daily  
711 mean values of wind speed and directions observed at the MIDAS station of Nyeri and with the daily mean values  
712 of wind speed and directions modelled by WRF in Nanyuki (Figure 8). The period between the 4<sup>th</sup> and the 10<sup>th</sup> of  
713 March, when the daily average concentrations of PM<sub>2.5</sub> observed in Nanyuki were around 2.2 µg m<sup>-3</sup> corresponds  
714 to higher wind speed conditions (between 4 and 5 m s<sup>-1</sup>) mainly coming from North-Est (around 60 degrees). In  
715 the same period, at Nyeri the modelled wind speed was low (between 1 and 2.5 m s<sup>-1</sup>) and mainly with a westerly  
716 component (between 220 and 300 degrees).

717  
718 In the periods of higher average daily concentrations of PM<sub>2.5</sub> between the 15<sup>th</sup> and the 19<sup>th</sup> and between 22<sup>nd</sup> and  
719 the 28<sup>th</sup> of February 2017, both in Nyeri (using observations) and in Nanyuki (using model outputs) the component  
720 of wind directions seems to be consistent in reproducing southern winds (between 120 and 190 degrees) with wind  
721 speeds between 1.5 and 2.5 m s<sup>-1</sup> in the first period and between 2 and 3 m s<sup>-1</sup> in the second period.

722  
 723  
 724  
 725  
 726  
 727  
 728  
 729  
 730  
 731

The correspondence between the wind speed and directions in particular time periods and the vicinity of the towns could suggest the potential dispersion of pollutants from the southern area where the hotspot of Nyeri is located upwind in the northern area of Nanyuki (downwind) in accordance with the wind fluxes from south to north from Nyeri from the observations and also from WRF outputs extracted from the Nanyuki location. The flux could also be driven by the location of Nyeri sited at the entrance of a basin between two mountain ranges. On the other hand, in the period of low concentrations between the 4<sup>th</sup> and the 10<sup>th</sup> of March northeaster winds (around 60 degrees) blow with high speed on Nanyuki (around 4 m s<sup>-2</sup>) while lower speed winds (between 1 and 2 m s<sup>-2</sup>) from a more variable directions (between 170 and 300 degrees) are blow in Nyeri preventing the possible dispersion of pollutants.



732  
 733  
 734  
 735  
 736

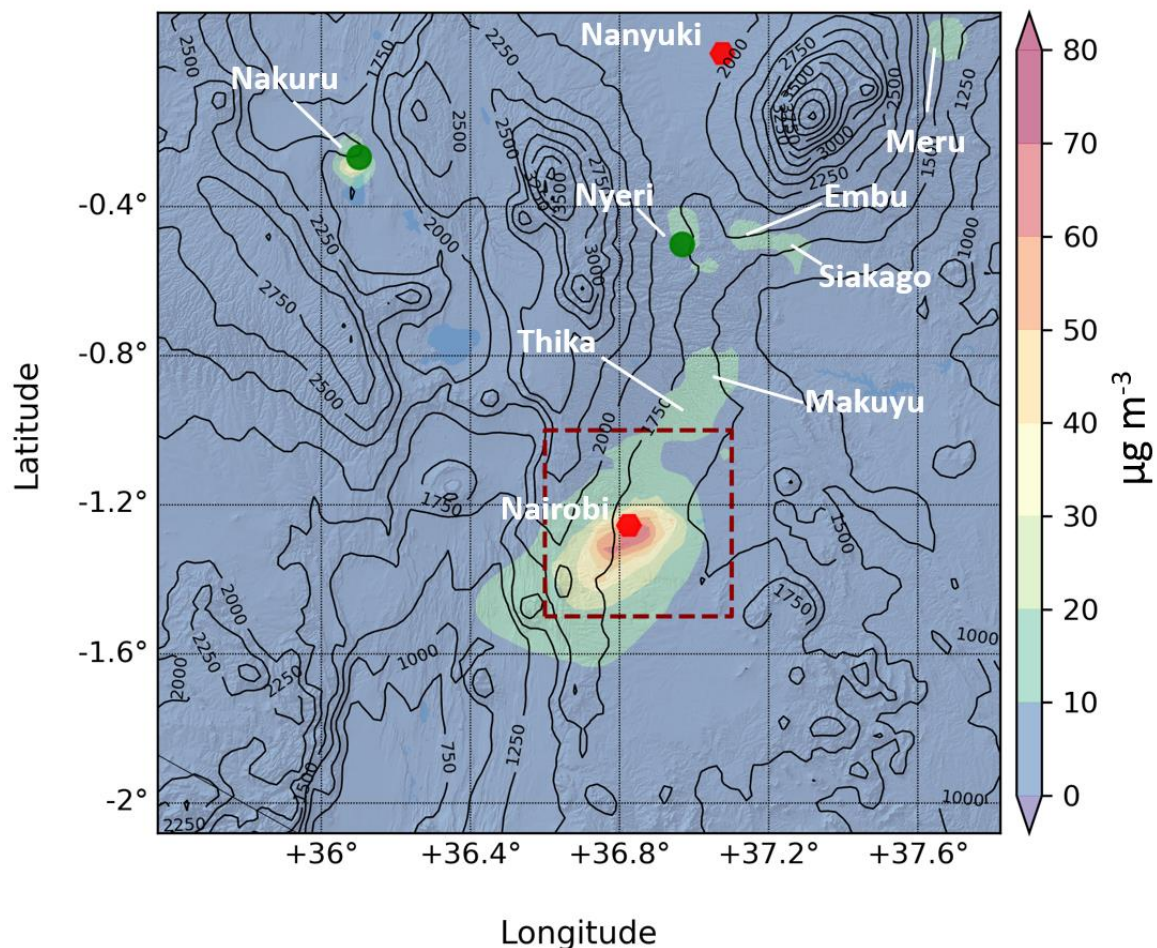
**Figure8:** Comparison between daily observed values of wind speed (grey spots) directions (grey lines) from the MIDAS site of Nyeri (n10 in Figure 3), modelled daily wind speed (blue dots) and directions (blue lines) from the site of Nanyuki with daily average observations of PM<sub>2.5</sub> (expressed in µg m<sup>-3</sup>, green columns) obtained from the sampling site of Nanyuki (red dot in Figure3c).

737  
 738  
 739  
 740  
 741  
 742  
 743  
 744  
 745  
 746  
 747  
 748

The present analysis was done on the relationships between weather conditions and the relative correspondence in hourly and daily levels of PM<sub>2.5</sub>. Further analyses are necessary to clarify the possible presence of additional or alternative factors influencing the changes in concentrations observed and modelled by CHIMERE. The presence of possible precipitations during the low concentration period could represent an alternative possibility the change in concentrations. Despite this no precipitation were recorded during that period according to Pope et al. (2018) and no precipitation was modelled by WRF in that time period. Nevertheless, the lack of additional weather observations in the sampling site of Nanyuki and middle way between the two towns prevent from any additional hypothesis in relation to the presence of possible pollutant transport phenomena that will be object of future investigations. Further efforts will be oriented in a more detailed trajectory analysis of the winds and in a more detailed representation of the emissive sources present in the area to investigate possible transport effects in this area.

749  
750  
751  
752  
753  
754  
755  
756  
757  
758  
759  
760  
761  
762

The average concentrations of PM<sub>2.5</sub> for the entire period of simulation between the 14<sup>th</sup> of February and 14<sup>th</sup> of March 2017 are shown for the domain centred over Kenya with spatial resolution of 2×2 km (KEN2K, Figure 9). Highest average concentrations during the monthly period are modelled in the urban area of Nairobi (defined by the red dashed square in Figure 9) with highest average values inside the city around 80 µg m<sup>-3</sup>. The concentrations are spread on average in the southwest area of the city and on the northeast side in direction of the conurbation of Thika and Makuyu. These towns became part of the Metropolitan Area of Nairobi in 2008 due to the rapid increase in population and urbanization of the area (UNEP, 2009) and represent a large hotspot of emissions of PM<sub>2.5</sub> with concentrations modelled between 20 and 30 µg m<sup>-3</sup> as average of the entire period. Other hotspots of concentration of PM<sub>2.5</sub> found in the domain are the city of Nakuru with average concentrations between 20 and 40 µg m<sup>-3</sup> and the area between Nyeri, Embu, Meru and Siakago with average concentrations around 20 and 30 µg m<sup>-3</sup> (Figure 9). The average of the modelled concentrations in the area of Nanyuki is generally smaller, with concentration not exceeding 10 µg m<sup>-3</sup> in the whole area.

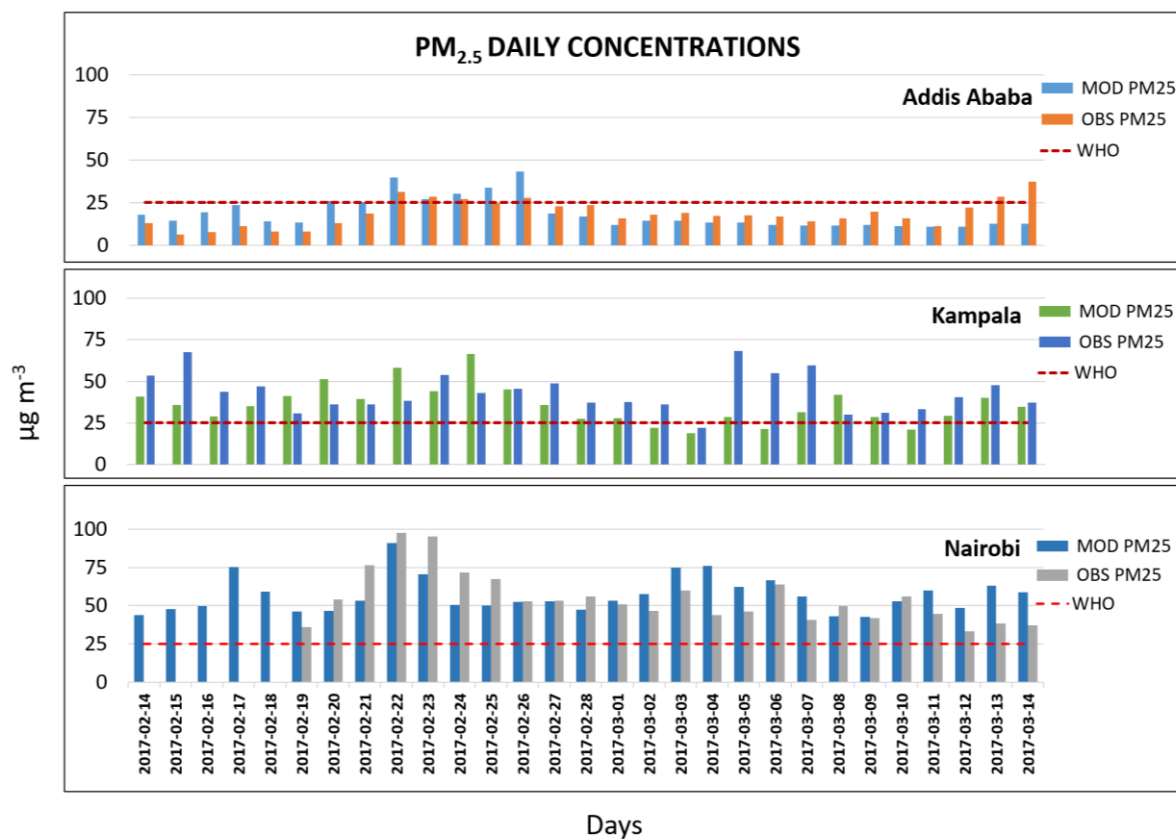


763  
764 **Figure 9:** Average concentration of PM<sub>2.5</sub> for the whole simulated period for the domain KEN2K at spatial resolution of 2×2  
765 km. The map shows the location of the hotspots with higher average concentrations modelled by CHIMERE for the entire  
766 period. The red dashed square shows the urban domain of Nairobi analysed for the Air Quality Indexes analysis in section  
767 3.3.

768 **3.3 CHIMERE as an Air Quality Management Tool**

769

770 The usefulness of CHIMERE as a decision support tool to facilitate air quality management of large urban  
 771 conurbations of SSEA was investigated for the three domains at a resolution of 2×2 km, namely: KEN2K, UGA2K  
 772 and ETH2K. Daily observations of PM<sub>2.5</sub> for the three domains were compared with modelled concentrations in  
 773 terms of number of exceedances from the WHO limit of 25 µg m<sup>-3</sup> observed and captured by the model (Figure  
 774 10). For the limited case of Nairobi, hourly average concentrations for the whole monitored period were compared  
 775 with Air Quality Indexes data and the spatial distribution of daily average concentrations on the constituencies  
 776 was analysed, highlighting how many areas of the city showed low air quality indexes during the analysed period  
 777 (Figure 11).



778

779 **Figure 10:** Daily concentrations of PM<sub>2.5</sub> between the 14<sup>th</sup> of February and 14<sup>th</sup> of March obtained from CHIMERE outputs  
 780 from domains at 2x2 km compared with US Embassy daily totals for the cities of Addis Ababa (top) and Kampala (middles)  
 781 and with ASAP observations for the city of Nairobi (bottom). All three simulations have been compared also with the WHO  
 782 threshold limit for PM<sub>2.5</sub> concentrations (red line). For the case of Nairobi, only observations from the 18<sup>th</sup> of February were  
 783 available.

784

785 Daily concentrations of PM<sub>2.5</sub> modelled by CHIMERE were compared with the number of exceedances of the  
 786 WHO limit (e.g., 25 µg m<sup>-3</sup>) observed during the simulated period. Figure 10 shows the daily average  
 787 concentrations for the three cities in the sampling sites used for the validation of the model. It can be seen that  
 788 Nairobi and Kampala have the highest number of exceedances from the WHO limits (24) followed by Addis  
 789 Ababa with only 6 observed exceedances. From Table 6 it can be seen that CHIMERE provides sufficient accuracy  
 790 to detect the exceedances of PM<sub>2.5</sub> from the WHO limits. In particular, it was able to detect 67 % of the exceedance

791 for Addis Ababa with only two false positives, 91 % for Kampala and all of the exceedances for Nairobi without  
 792 any false positives.

793  
 794 The Air Quality Index (AQI) represents the conversion of concentrations for fine particles such as PM<sub>2.5</sub> to a  
 795 number on a scale from 0 to 500 (Table 7). The higher the AQI value, the greater the level of air pollution and the  
 796 greater the health concern. AQI values at or below 100 are generally thought of as satisfactory. When AQI values  
 797 are above 100, air quality is unhealthy: at first for certain sensitive groups of people (101 – 150), then for everyone  
 798 as AQI values get higher (> 151) (EPA, 2012).

799

800 **Table 6:** Summary of the number of WHO exceeding limits for PM<sub>2.5</sub> during the simulated period from the 14<sup>th</sup> of February to  
 801 the 14<sup>th</sup> of March 2017 observed and modelled. Ratio between the observed and modelled Exceeding limit and number of  
 802 model overestimations are also reported.

Domains	WHO Exceeding Limits (obs)	WHO Exceeding Limits (mod)	Ratio (%)	Model False positive
Nairobi	24	24	100	0
Addis Ababa	6	4	67	2
Kampala	24	22	91	0

803

804 The daily average concentrations of PM<sub>2.5</sub> during the analysed period between the 14<sup>th</sup> of February and 14<sup>th</sup> of  
 805 March 2017 have been averaged for the urban area of Nairobi (red square in Figure 9 and Figure 11) and compared  
 806 with the city constituencies spatial extension according to data from the Open Africa dataset (Open-Africa, 2018).  
 807 According to the division, 17 are the constituencies inside the Nairobi city boundaries (Figure 11). Averaged daily  
 808 concentrations of PM<sub>2.5</sub> show that 8 of 17 constituencies had AQI values between 55.5 - 150.4 µg m<sup>-3</sup> during the  
 809 whole period. These areas are the most central and urbanized of Nairobi. Starehe constituency (n13 in Figure 11)  
 810 contains the Tom Mboya Street sampling site (black spot in Figure 11) previously discussed where the WHO  
 811 limits for PM<sub>2.5</sub> have been systematically exceeded during the analysed period. According to the SEDAC  
 812 population density data this area has population density between 15,000 and 30,000 people/km<sup>2</sup> exposed to AQI  
 813 between 151-200 corresponding to unhealthy category for human health. Finally, the Langata constituency  
 814 (magenta spot in Figure 11) has a population of 176,000 people and shows average levels of PM<sub>2.5</sub> of 45 µg m<sup>-3</sup>,  
 815 unhealthy for sensitive groups of people.

816

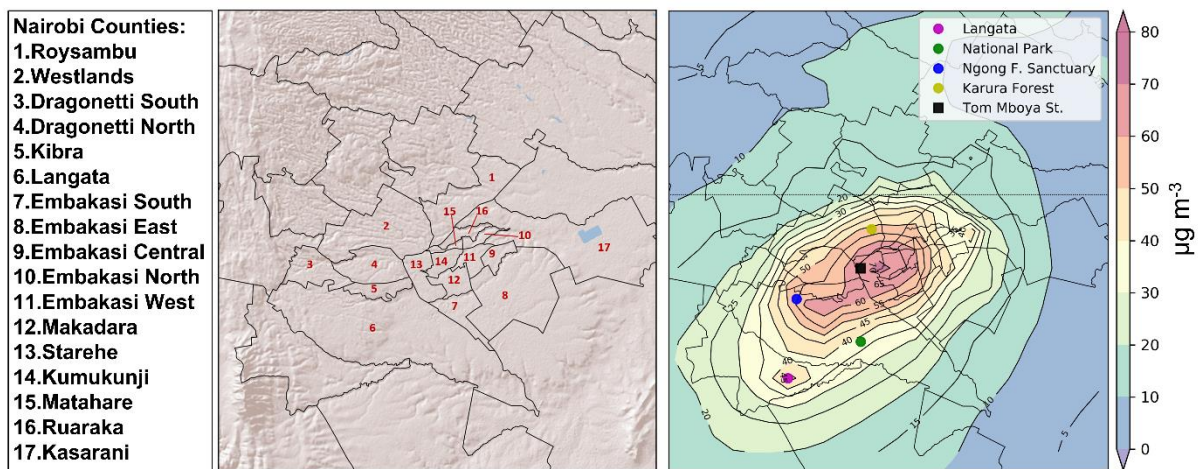
817 **Table 7:** Air Quality Index categories and relative range of 24-hour average concentrations for PM<sub>2.5</sub> reported by the US  
 818 EPA revised air quality standard for particle pollution of 2012 (EPA, 2012)

AQI Category	Index values	AQI Breakpoints (µg m <sup>-3</sup> on 24-hour average)
Good	0 - 50	0.0 - 12.0
Moderate	51 - 100	12.1 - 35.4
Unhealthy for sensitive Groups	101 - 150	35.5 - 55.4
Unhealthy	151 - 200	55.5 - 150.4
Very Unhealthy	201 - 300	150.5 - 250.4
Hazardous	>301	>250.5

819

820 Moreover, Nairobi has a number of natural areas on the outskirts of city. Some particular locations such as the  
 821 Karura Forest (yellow spot in Figure 11) and the Ngong Forest Sanctuary (blue spot in Figure 11) show averaged  
 822 daily levels of PM<sub>2.5</sub> around 50 and 55 µg m<sup>-3</sup> corresponding to an AQI of between 101 and 150 (e.g., unhealthy

823 for certain sensitive groups of people). According to SEDAC data, the population density is between 10,000 and  
 824 15,000 people/km<sup>2</sup> in this area. Similarly, in the south side, near the entrance to the Nairobi National Park (1.36°  
 825 S, 36.82° E, green spot in Figure 11) the average daily levels of PM<sub>2.5</sub> are approximately 40 µg m<sup>-3</sup> with AQI  
 826 values between 101 and 150 with a population density around 10,000 people/km<sup>2</sup>. This area (surface area 117  
 827 km<sup>2</sup>) has been impacted by a rapid urbanization since 1973 with a consequent increase of human activities  
 828 including settlement, pastoralism and agriculture (Ogega O.M., 2019). These activities have already made it  
 829 difficult for wildlife to migrate to and from the Nairobi National Park also are resulting in a deterioration of air  
 830 quality. The rapid increase of population density in the south side of Nairobi seriously risk increasing the level or  
 831 AQI exposing more people to harmful level of PM<sub>2.5</sub>.  
 832



833  
 834 **Figure 11:** Map showing the urban area of the city of Nairobi shown as dashed square in Figure 9. The constituency division  
 835 of Nairobi (left) from Open Africa dataset (Open Africa, 2018) is compared with the average hourly concentrations of PM<sub>2.5</sub>  
 836 over the analysed period (right).  
 837

838 **4 Conclusions**

839  
 840 The WRF and CHIMERE models were configured and validated to simulate the air quality levels of PM in Eastern  
 841 Sub-Saharan African urban conurbations.

842  
 843 In order to obtain updated anthropogenic emissions for 2017, the global EDGAR inventory and the DICE  
 844 inventory for Africa were merged and spatially distributed using population density data for the year 2017  
 845 obtained by linear extrapolation.

846  
 847 WRF showed a variable capability in reproducing the main surface weather patterns according to the different  
 848 conditions of the three domains. A lower agreement between observations and the model was observed in Kampala  
 849 for relative humidity and wind speed. The analysis was carried out on all surface meteorological stations available  
 850 from the MIDAS network on a three-hourly basis. A further meteorological analysis extended to vertical profiles  
 851 could reveal possible limitations of the model. However, the absence of vertical meteorological data limited the  
 852 analysis and validation to ground level only.

853

854 CHIMERE was able to reproduce the daily levels of PM<sub>2.5</sub> for the urban site of Nairobi as well as for the rural site  
855 of Nanyuki. The 69 % of the MFB values and 88 % of the MFE value were inside the highest confidence area for  
856 Nairobi and the 97 % and 99 % for Nanyuki attesting that the agreement between the observed and modelled data  
857 was sufficient to allow for quantitative analyses of daily average concentrations. Similar findings were also found  
858 for the other two urban background domains of Addis Ababa (57 % for MFB and 80 % for MFE) and Kampala  
859 (48% for MFB and 74 % for MFE) despite different characteristics and sources of observation being used for the  
860 validation. The discrepancies observed in the hourly trends of PM<sub>2.5</sub> modelled by CHIMERE compared to  
861 observed values in the urban sites suggest that further studies are needed in the three urban areas. These studies  
862 are required to improve the understanding of the typology and quantity of local emission sources, which are  
863 sometimes misrepresented or absent in global emission inventories. This will enable the chemical processes acting  
864 in the urban troposphere to be adequately characterised and thereby actual air quality levels to be determined.

865

866 Nevertheless, using existing data sets, CHIMERE has shown reliability in reproducing both hourly and daily levels  
867 of PM<sub>2.5</sub> with hourly values largely inside the range of reliability connected with mean fractional bias and error.  
868 The merged emission inventory DICE-EDGAR, despite the low resolution was able to return a correct magnitude  
869 for the emissions in representation of urban and rural context. Despite this, few urban peaks observed in Nairobi  
870 have been missed by CHIMERE or in other cases misrepresented highlighting the necessity of further efforts in  
871 the creation of newer emission inventories for SSEA. In the light of this, the possibility to develop local emission  
872 inventories, ideally at high spatial resolution it would represent a significant step ahead in the air quality research  
873 in this area of the world. Despite this and at the extent of the present data, CHIMERE showed enough robustness  
874 and reliability to be adopted as a decision support tool for the management of air quality, correctly reproducing  
875 most of the exceedances of the limits set by the WHO for PM<sub>2.5</sub> for all three cities considered.

876

877 The analysis focused on the average concentrations of PM<sub>2.5</sub> for the domain of Kenya revealed that the  
878 metropolitan area of Nairobi represents a big hotspot of air pollution but that also small cities located in the  
879 outskirts of the capital of Kenya showed worrying levels of atmospheric contamination. These levels of air  
880 pollution have the potential capability to affect also rural areas where the local emissions are rare or not present.  
881 The possibility of transport phenomena of PM<sub>2.5</sub> towards these areas, however, is still to be verified. The work  
882 has also shown for urban area of Nairobi the presence of low and unhealthy air quality indexes in 8 of 17 its  
883 constituencies and the relative population density exposed to harmful level of air contamination. Moreover, a  
884 number of natural areas in the outskirts of Nairobi have similarly low levels of AQI and increasing population  
885 highlighting how the problem of poor urban air quality due to rapid urbanisation, anthropogenic activities and  
886 lack of regulation can also detrimentally affect and deteriorate natural habitats.

887

888 Future efforts to improve the calibration and validation of the modelling system, especially relating to  
889 meteorology, will focus on assessing the dispersion dynamics of contaminants through urban centres and possible  
890 pollution transport events from urban to rural areas. To aid this, further work is required by local East African  
891 authorities and research bodies to improve the quantity and the quality of data for weather and air quality  
892 simulations. However, in this work, we have shown that currently available data is sufficient to carry out

893 simulations of air quality that can be used for quantitative evaluation of anthropogenic emissions impact and to  
894 support mitigation policies at the local level.

895

896 **Authors Contribution: Andrea Mazzeo:** Conceptualization, Methodology, Software, Validation, Writing-  
897 Original draft preparation, Writing- Reviewing and Editing. **Michael Burrow:** Supervision, Writing - Review &  
898 Editing **Andrew Quinn:** Supervision, Resources. **Eloise A. Marais:** Data curation, Resources, Writing - Review  
899 and Editing. **Ajit Singh:** Resources, **David N'gang'a:** Resources, **Michael Gatari:** Resources. **Francis Pope:**  
900 Supervision, Data curation, Funding acquisition, Writing - Review and Editing.

901

#### 902 **Acknowledgements:**

903 The work is funded by the UK Department for International Development (DFID) via the EPSRC grant 'Digital  
904 Air Quality' (EP/T030100/1) and by the East Africa Research Fund (EARF) grant 'A Systems Approach to Air  
905 Pollution (ASAP) East Africa'. The practical support of the Schools of Geography and Earth Sciences and  
906 Engineering at the University of Birmingham are gratefully acknowledged.

907

908 **Data Availability:** the combined DICE-EDGAR anthropogenic emission inventory is downloadable from:  
909 <https://doi.org/10.25500/edata.bham.00000695>

910

#### 911 **References**

912 Alduchov O., E. R.: Improved Magnus Form Approximation of Saturation Vapor Pressure, *J. Of Appl. Met.*, 35,  
913 601-609, [https://doi.org/10.1175/1520-0450\(1996\)035<0601:IMFAOS>2.0.CO;2](https://doi.org/10.1175/1520-0450(1996)035<0601:IMFAOS>2.0.CO;2), 1996.

914 Amegah, A. K., and Agyei-Mensah, S.: Urban air pollution in Sub-Saharan Africa: Time for action, *Environ*  
915 *Pollut*, 220, 738-743, 10.1016/j.envpol.2016.09.042, 2017.

916 Anav, A., Menut, L., Khvorostyanov, D., and VÍOvy, N.: Impact of tropospheric ozone on the Euro-  
917 Mediterranean vegetation, *Global Change Biology*, 17, 2342-2359, 10.1111/j.1365-2486.2010.02387.x, 2011.

918 Assamoi, E.-M., and Liousse, C.: A new inventory for two-wheel vehicle emissions in West Africa for 2002,  
919 *Atmospheric Environment*, 44, 3985-3996, 10.1016/j.atmosenv.2010.06.048, 2010.

920 Avis W. and Khaemba W.: Vulnerability and air pollution, 2018.

921 Barnard, J.: An evaluation of the FAST-J photolysis algorithm for predicting nitrogen dioxide photolysis rates  
922 under clear and cloudy sky conditions, *Atmospheric Environment*, 38, 3393-3403,  
923 10.1016/j.atmosenv.2004.03.034, 2004.

924 Bessagnet, B., Pirovano, G., Mircea, M., Cuvelier, C., Aulinger, A., Calori, G., Ciarelli, G., Manders, A., Stern,  
925 R., Tsyro, S., García Vivanco, M., Thunis, P., Pay, M.-T., Colette, A., Couvidat, F., Meleux, F., Rouil, L., Ung,  
926 A., Aksoyoglu, S., Baldasano, J. M., Bieser, J., Briganti, G., Cappelletti, A., D'Isidoro, M., Finardi, S.,  
927 Kranenburg, R., Silibello, C., Carnevale, C., Aas, W., Dupont, J.-C., Fagerli, H., Gonzalez, L., Menut, L.,  
928 Prévôt, A. S. H., Roberts, P., and White, L.: Presentation of the EURODELTA III intercomparison exercise –  
929 evaluation of

930 the chemistry transport models' performance on criteria pollutants and joint

931 analysis with meteorology, *Atmospheric Chemistry and Physics*, 16, 12667-12701, 10.5194/acp-16-12667-  
932 2016, 2016.

933 Bian, H., Prather, M.: Fast-J2: accurate simulation of stratospheric photolysis in global chemical models, *J.*  
934 *Atmos. Chem*, 41, 281–296, <https://doi.org/10.1023/A:1014980619462>, 2002.

935 Bockarie, A. S., Marais, E. A., and MacKenzie, A. R.: Air Pollution and Climate Forcing of the Charcoal  
936 Industry in Africa, *Environ Sci Technol*, 54, 13429-13438, 10.1021/acs.est.0c03754, 2020.

937 Boylan, J. W., and Russell, A. G.: PM and light extinction model performance metrics, goals, and criteria for  
938 three-dimensional air quality models, *Atmospheric Environment*, 40, 4946-4959,  
939 10.1016/j.atmosenv.2005.09.087, 2006.

940 Brauer, M., Amann, M., Burnett, R. T., Cohen, A., Dentener, F., Ezzati, M., Henderson, S. B., Krzyzanowski,  
941 M., Martin, R. V., Van Dingenen, R., van Donkelaar, A., and Thurston, G. D.: Exposure assessment for

942 estimation of the global burden of disease attributable to outdoor air pollution, *Environ Sci Technol*, 46, 652-  
943 660, 10.1021/es2025752, 2012.

944 Carter, W. P. L.: Development of the SAPRC-07 chemical mechanism, *Atmospheric Environment*, 44, 5324-  
945 5335, 10.1016/j.atmosenv.2010.01.026, 2010.

946 Collins, W., Rasch, P., Boville, B., Hack, J., McCaa, J., Williamson, D., Kiehl, J., Briegleb, B., : Description of  
947 the NCAR Community Atmosphere Model (CAM 3.0). , NCAR Tech Notes, 2004.

948 Crippa M., G. D., Muntean M., Shaaf E., Dentener F., van Aardenne J.A., Monni S., Doering U., Olivier J.G.J.,  
949 Pagliari V. and Janssens-Maenhout G.: Gridded emissions of air pollutants for the period 1970-2012 within  
950 EDGAR v4.3.2, *Earth Sci. Data*, 10, 1987 – 2013, <https://doi.org/10.5194/essd-2018-31>, 2018.

951 Dalal, S., Beunza, J. J., Volmink, J., Adebamowo, C., Bajunirwe, F., Njelekela, M., Mozaffarian, D., Fawzi, W.,  
952 Willett, W., Adami, H. O., and Holmes, M. D.: Non-communicable diseases in sub-Saharan Africa: what we  
953 know now, *Int J Epidemiol*, 40, 885-901, 10.1093/ije/dyr050, 2011.

954 deSouza P., N. V., Klopp J. M., Shaw B. E., Ho W. O., Saffell J., Jones R. and Ratti C.: : A Nairobi experiment  
955 in using low cost air quality monitors, *Clean Air Journal*, 27, 12-42, <http://dx.doi.org/10.17159/2410-972X/2017/v27n2a6>, 2017.

957 Egondi, T., Kyobutungi, C., Ng, N., Muindi, K., Oti, S., van de Vijver, S., Ettarh, R., and Rocklov, J.:  
958 Community perceptions of air pollution and related health risks in Nairobi slums, *Int J Environ Res Public*  
959 *Health*, 10, 4851-4868, 10.3390/ijerph10104851, 2013.

960 Guidance for regulatory application of the urban airshed model UAM, 1991.

961 Revised Air Quality Standards for particle pollution and updates to the Air Quality Index (AQI):  
962 [https://www.epa.gov/sites/production0-etrfvgy8ufiles/2016-04/documents/2012\\_aqi\\_factsheet.pdf](https://www.epa.gov/sites/production0-etrfvgy8ufiles/2016-04/documents/2012_aqi_factsheet.pdf) 2012.

963 Gaita, S. M., Boman, J., Gatari, M. J., Pettersson, J. B. C., and Janhäll, S.: Source apportionment and seasonal  
964 variation of PM<sub>2.5</sub> in a Sub-Saharan African city: Nairobi, Kenya, *Atmospheric Chemistry and*  
965 *Physics*, 14, 9977-9991, 10.5194/acp-14-9977-2014, 2014.

966 Gatari, M. J., Kinney, P. L., Yan, B., Sclar, E., Volavka-Close, N., Ngo, N. S., Mwaniki Gaita, S., Law, A.,  
967 Ndiba, P. K., Gachanja, A., Graeff, J., and Chillrud, S. N.: High airborne black carbon concentrations measured  
968 near roadways in Nairobi, Kenya, *Transportation Research Part D: Transport and Environment*, 68, 99-109,  
969 10.1016/j.trd.2017.10.002, 2019.

970 Guenther, A., Karl, T., Harley, P., Wiedinmyer, C., Palmer, P., and Geron, C.: : Estimates of global terrestrial  
971 isoprene emissions using MEGAN (Model of Emissions of Gases and Aerosols from Nature), *Atmos. Chem.*  
972 *Phys*, 6, 3181–3210, <https://hal.archives-ouvertes.fr/hal-00295995>, 2006.

973 Hauglustaine, D. A., Hourdin, F., Jourdain, L., Filiberti, M. A., Walters, S., Lamarque, J. F., and Holland, E. A.:  
974 Interactive chemistry in the Laboratoire de Météorologie Dynamique general circulation model: Description and  
975 background tropospheric chemistry evaluation, *Journal of Geophysical Research: Atmospheres*, 109, n/a-n/a,  
976 10.1029/2003jd003957, 2004.

977 Haywood, J. M., Pelon, J., Formenti, P., Bharmal, N., Brooks, M., Capes, G., Chazette, P., Chou, C.,  
978 Christopher, S., Coe, H., Cuesta, J., Derimian, Y., Desboeufs, K., Greed, G., Harrison, M., Heese, B.,  
979 Highwood, E. J., Johnson, B., Mallet, M., Marticorena, B., Marsham, J., Milton, S., Myhre, G., Osborne, S. R.,  
980 Parker, D. J., Rajot, J. L., Schulz, M., Slingo, A., Tanré, D., and Tulet, P.: Overview of the Dust and Biomass-  
981 burning Experiment and African Monsoon Multidisciplinary Analysis Special Observing Period-0, *Journal of*  
982 *Geophysical Research*, 113, 10.1029/2008jd010077, 2008.

983 Hong S., D. J., and Shu–Hua Chen S.: A revised approach to ice microphysical processes for the bulk  
984 parameterization of clouds and precipitation, *Mon. Wea. Rev.*, 132, 103-120,  
985 [https://journals.ametsoc.org/view/journals/mwre/132/1/1520-0493\\_2004\\_132\\_0103\\_aratim\\_2.0.co\\_2.xml](https://journals.ametsoc.org/view/journals/mwre/132/1/1520-0493_2004_132_0103_aratim_2.0.co_2.xml), 2004.

986 Hong S., N. Y., Dudhia J.: : A new vertical diffusion package with an explicit treatment of entrainment  
987 processes, *Mon. Wea. Rev.*, 134, 2318–2341,  
988 <https://journals.ametsoc.org/view/journals/mwre/134/9/mwr3199.1.xml>, 2006.

989 Kerandi, N., Arnault, J., Laux, P., Wagner, S., Kitheka, J., and Kunstmann, H.: Joint atmospheric-terrestrial  
990 water balances for East Africa: a WRF-Hydro case study for the upper Tana River basin, *Theoretical and*  
991 *Applied Climatology*, 131, 1337-1355, 10.1007/s00704-017-2050-8, 2017.

992 Kerandi, N. M., Laux, P., Arnault, J., and Kunstmann, H.: Performance of the WRF model to simulate the  
993 seasonal and interannual variability of hydrometeorological variables in East Africa: a case study for the Tana  
994 River basin in Kenya, *Theoretical and Applied Climatology*, 130, 401-418, 10.1007/s00704-016-1890-y, 2016.

995 Kinney, P. L., Gichuru, M. G., Volavka-Close, N., Ngo, N., Ndiba, P. K., Law, A., Gachanja, A., Gaita, S. M.,  
996 Chillrud, S. N., and Sclar, E.: Traffic Impacts on PM(2.5) Air Quality in Nairobi, Kenya, *Environ Sci Policy*,  
997 14, 369-378, 10.1016/j.envsci.2011.02.005, 2011.

998 Kume, A., Charles, K., Berehane, Y., Anders, E. and Ali, A.: Magnitude and variation of traffic air pollution as  
999 measured by CO in the City of Addis Ababa, Ethiopia, *Ethiopian Journal of Health Development*, 24,  
1000 <https://doi.org/10.4314/ejhd.v24i3.68379>, 2010.

1001 Lacaux, J. P., Brustet, J.M., Delmas, R. et al.: Biomass burning in the tropical savannas of Ivory Coast: An  
1002 overview of the field experiment Fire of Savannas (FOS/DECAFE 91), *J Atmos Chem*, 22, 195–216,  
1003 <https://doi.org/10.1007/BF00708189>, 1995.

1004 Li, C., Martin, R. V., van Donkelaar, A., Boys, B. L., Hammer, M. S., Xu, J. W., Marais, E. A., Reff, A., Strum,  
1005 M., Ridley, D. A., Crippa, M., Brauer, M., and Zhang, Q.: Trends in Chemical Composition of Global and  
1006 Regional Population-Weighted Fine Particulate Matter Estimated for 25 Years, *Environ Sci Technol*, 51, 11185-  
1007 11195, 10.1021/acs.est.7b02530, 2017.

1008 Lioussé, C., Guillaume, B., Grégoire, J. M., Mallet, M., Galy, C., Pont, V., Akpo, A., Bedou, M., Castéra, P.,  
1009 Dungall, L., Gardrat, E., Granier, C., Konaré, A., Malavelle, F., Mariscal, A., Mieville, A., Rosset, R., Serça, D.,  
1010 Solmon, F., Tummon, F., Assamoi, E., Yoboué, V., and Van Velthoven, P.: Updated African biomass burning  
1011 emission inventories in the framework of the AMMA-IDAF program, with an evaluation of combustion  
1012 aerosols, *Atmospheric Chemistry and Physics*, 10, 9631-9646, 10.5194/acp-10-9631-2010, 2010.

1013 Lioussé, C., Assamoi, E., Criqui, P., Granier, C., & Rosset, R.: Explosive growth in African combustion  
1014 emissions from 2005 to 2030, *Environmental Research Letters*, 9, <https://doi.org/10.1088/1748-9326/9/3/035003>, 2014.

1015

1016 Loosmore, G. A., and Cederwall, R. T.: Precipitation scavenging of atmospheric aerosols for emergency  
1017 response applications: testing an updated model with new real-time data, *Atmospheric Environment*, 38, 993-  
1018 1003, <https://doi.org/10.1016/j.atmosenv.2003.10.055>, 2004.

1019 Mailler, S., Menut, L., Khvorostyanov, D., Valari, M., Couvidat, F., Siour, G., Turquety, S., Briant, R.,  
1020 Tuccella, P., Bessagnet, B., Colette, A., Létinois, L., Markakis, K., and Meleux, F.: CHIMERE-2017: from  
1021 urban to hemispheric chemistry-transport modeling, *Geoscientific Model Development*, 10, 2397-2423,  
1022 10.5194/gmd-10-2397-2017, 2017.

1023 Marais, E. A., and Wiedinmyer, C.: Air Quality Impact of Diffuse and Inefficient Combustion Emissions in  
1024 Africa (DICE-Africa), *Environ Sci Technol*, 50, 10739-10745, 10.1021/acs.est.6b02602, 2016.

1025 Marais, E. A., Silvern, R. F., Vodonos, A., Dupin, E., Bockarie, A. S., Mickley, L. J., and Schwartz, J.: Air  
1026 Quality and Health Impact of Future Fossil Fuel Use for Electricity Generation and Transport in Africa, *Environ*  
1027 *Sci Technol*, 53, 13524-13534, 10.1021/acs.est.9b04958, 2019.

1028 Markakis, K., Valari, M., Perrussel, O., Sanchez, O., and Honore, C.: Climate-forced air-quality modeling at the  
1029 urban scale: sensitivity to model resolution, emissions and meteorology, *Atmospheric Chemistry and Physics*,  
1030 15, 7703-7723, 10.5194/acp-15-7703-2015, 2015.

1031 Mazzeo, A., Huneus, N., Ordoñez, C., Orfanoz-Cheuquelaf, A., Menut, L., Mailler, S., Valari, M., van der  
1032 Gon, H. D., Gallardo, L., and Muñoz, R.: Impact of residential combustion and transport emissions on air  
1033 pollution in Santiago during winter, *Atmospheric Environment*, 190, 195-208, 2018.

1034 Mbewu, A., Mbanya, J.C., : Disease and Mortality in Sub-Saharan Africa, in: *Cardiovascular disease* edited by:  
1035 Bank, W., 2006.

1036 Nenes, A., Pilinis, C., Pandis, S.: : Isorropia: a new thermodynamic model for inorganic multicomponent  
1037 atmospheric aerosols., *Aquat. Geochem*, 4, 123-152, <https://doi.org/10.1023/A:1009604003981>, 1998.

1038 Ngo, N. S., Gatari, M., Yan, B., Chillrud, S. N., Bouhamam, K., and Kinney, P. L.: Occupational exposure to  
1039 roadway emissions and inside informal settlements in sub-Saharan Africa: A pilot study in Nairobi, Kenya,  
1040 *Atmos Environ* (1994), 111, 179-184, 10.1016/j.atmosenv.2015.04.008, 2015.

1041 Ogega O.M., W. H. N., Mbugua J: Exploring the Future of Nairobi National Park in a Changing Climate and  
1042 Urban Growth., in: *The Geography of Climate Change Adaptation in Urban Africa.*, edited by: Macmillan, P.,  
1043 2019.

1044 <https://open.africa/dataset/kenya-administrative-boundaries/resource/b5bee56d-b7cb-4f23-8f2b-356ca0044bf3>,  
1045 2018.

1046 Pai, S. J., Heald, C. L., Pierce, J. R., Farina, S. C., Marais, E. A., Jimenez, J. L., Campuzano-Jost, P., Nault, B.  
1047 A., Middlebrook, A. M., Coe, H., Shilling, J. E., Bahreini, R., Dingle, J. H., and Vu, K.: An evaluation of global  
1048 organic aerosol schemes using airborne observations, *Atmospheric Chemistry and Physics*, 20, 2637-2665,  
1049 10.5194/acp-20-2637-2020, 2020.

1050 Parkin, D. M., Sitas, F., Chirenje, M., Stein, L., Abratt, R., and Wabinga, H.: Part I: Cancer in Indigenous  
1051 Africans—burden, distribution, and trends, *The Lancet Oncology*, 9, 683-692, 10.1016/s1470-2045(08)70175-x,  
1052 2008.

1053 Peña, M. a. R., A.: Environmental Exposures and Cardiovascular Disease, *Cardiology clinics*, 35, 71-86,  
1054 <https://doi.org/10.1016/j.ccl.2016.09.001>, 2017.

1055 Petkova, E. P., Jack, D. W., Volavka-Close, N. H., and Kinney, P. L.: Particulate matter pollution in African  
1056 cities, *Air Quality, Atmosphere and Health*, 6, 603-614, <https://doi.org/10.1007/s11869-013-0199-6>, 2013.

1057 Pohl, B., Crétat, J., and Camberlin, P.: Testing WRF capability in simulating the atmospheric water cycle over  
1058 Equatorial East Africa, *Climate Dynamics*, 37, 1357-1379, 10.1007/s00382-011-1024-2, 2011.

1059 Pope, F. D., Gatari, M., Ng'ang'a, D., Poynter, A., and Blake, R.: Airborne particulate matter monitoring in  
1060 Kenya using calibrated low-cost sensors, *Atmospheric Chemistry and Physics*, 18, 15403-15418, 10.5194/acp-  
1061 18-15403-2018, 2018.

1062 Powers, J. G., Klemp, J.B., Skamarock, W.C., Davis, C.A., Dudhia, J., Gill, D.O., Coen, J.L., Gochis, D.J., Ah  
1063 madov, R., Peckham, S.E., Grell, G.A., Michalakes, J., Trahan, S., Benjamin, S.G., Alexander, C.R., Di mego,  
1064 G.J., Wang, W., Schwartz, C.S., Romine, G.S., Liu, Z., Snyder, C., Chen, F., Barlage, M.J., Yu, W., Duda,  
1065 M.G.: : The weather research and forecasting model: overview, system efforts, and future directions, *Bull. Am.*  
1066 *Meteorol. Soc.*, 98, 1717–1737, <https://doi.org/10.1175/BAMS-D-15-00308.1>, 2017.

1067 Pun, B. K., Seigneur, C., and Lohman, K.: Modeling secondary organic aerosol formation via multiphase  
1068 partitioning with molecular data, *Environ. Sci. Technol.*, 40, 4722–4731, <https://doi.org/10.1021/es0522736>,  
1069 2006.

1070 Real, E., and Sartelet, K.: Modeling of photolysis rates over Europe: impact on chemical gaseous species and  
1071 aerosols, *Atmospheric Chemistry and Physics*, 11, 1711-1727, 10.5194/acp-11-1711-2011, 2011.

1072 Schwander, S., Okello, C. D., Freers, J., Chow, J. C., Watson, J. G., Corry, M., and Meng, Q.: Ambient  
1073 particulate matter air pollution in Mpererwe District, Kampala, Uganda: a pilot study, *J Environ Public Health*,  
1074 2014, 763934, 10.1155/2014/763934, 2014.

1075 Seinfeld, J. H., Pandis, S.N.: *Atmospheric chemistry and physics: from air pollution to climate change*, edited  
1076 by: Sons, J. W., 2016.

1077 Singh, A., Avis, W. R., and Pope, F. D.: Visibility as a proxy for air quality in East Africa, *Environmental*  
1078 *Research Letters*, 15, 10.1088/1748-9326/ab8b12, 2020.

1079 Singh, A., Ng'ang'a, D., Gatari, M., Kidane, A. W., Alemu, Z., Derrick, N., Webster, M. J., Bartington, S.,  
1080 Thomas, N., Avis, W. R., and Pope, F.: Air quality assessment in three East African cities using calibrated low-  
1081 cost sensors with a focus on road-based hotspots, *Environmental Research Communications*, 10.1088/2515-  
1082 7620/ac0e0a, 2021.

1083 Skamarock, W., Klemp, J., Dudhia, J., Gill, D., Barker, D., Duda, M., Huang, X., Wang, W., Powers, J., : A  
1084 description of the advanced research WRF version 3. NCAR, 2008.

1085 Teklay, A., Dile, Y. T., Asfaw, D. H., Bayabil, H. K., and Sisay, K.: Impacts of land surface model and land use  
1086 data on WRF model simulations of rainfall and temperature over Lake Tana Basin, Ethiopia, *Heliyon*, 5,  
1087 e02469, 10.1016/j.heliyon.2019.e02469, 2019.

1088 Telford, P. J., Abraham, N. L., Archibald, A. T., Braesicke, P., Dalvi, M., Morgenstern, O., O'Connor, F. M.,  
1089 Richards, N. A. D., and Pyle, J. A.: Implementation of the Fast-JX Photolysis scheme (v6.4) into the UKCA  
1090 component of the MetUM chemistry-climate model (v7.3), *Geoscientific Model Development*, 6, 161-177,  
1091 10.5194/gmd-6-161-2013, 2013.

1092 Tewari, M., F. Chen, W. Wang, J. Dudhia, M. A. LeMone, K. Mitchell, M. Ek, G. Gayno, J. Wegiel, and R. H.  
1093 Cuenca.: Implementation and verification of the unified NOAA land surface model in the WRF model.  
1094 In *Proceedings of the 20th Conference on Weather Analysis and Forecasting, 16th Conference on Numerical*  
1095 *Weather Prediction*, Seattle, 2004.

1096 Thompson A. M., W. J. C., Hudson R. D., Guo H., Herman J. R., and Fujiwara M.: Tropical tropospheric ozone  
1097 and biomass burning Science, 291, 2128-2132, 10.1126/science.291.5511.2128, 2001.

1098 Trewhela, B., Huneus, N., Munizaga, M., Mazzeo, A., Menut, L., Mailler, S., Valari, M., and Ordoñez, C.:  
1099 Analysis of exposure to fine particulate matter using passive data from public transport, *Atmospheric*  
1100 *Environment*, 215, 116878, 2019.

1101 UK, M. O.: Met Office Integrated Data Archive System (MIDAS) Land and Marine Surface Stations Data  
1102 (1853-current). NCAS British At-mospheric Data Centre, date of citation. UK, M. O. (Ed.), 2012.

1103 New Urban Agenda <http://habitat3.org/wp-content/uploads/NUA-English.pdf>, 2017.

1104 City of Nairobi Environment Outlook: <https://wedocs.unep.org/handle/20.500.11822/8738>, 2009.

1105 FEWS NET: <https://fews.net/east-africa/seasonal-monitor/march-2022>, access: May 2022, 2022.

1106 Valari, M., and Menut, L.: Transferring the heterogeneity of surface emissions to variability in pollutant  
1107 concentrations over urban areas through a chemistry-transport model, *Atmospheric Environment*, 44, 3229-  
1108 3238, 10.1016/j.atmosenv.2010.06.001, 2010.

1109 Van Leer, B.: Towards the ultimate conservative difference scheme. V. A second-order sequel to Godunov's  
1110 method. , *Journal of Computational Physics*, 32, 101–136, 10.1016/0021-9991(79)90145-1, 1979.

1111 van Loon, M., Vautard, R., Schaap, M., Bergström, R., Bessagnet, B., Brandt, J., Builtjes, P. J. H., Christensen,  
1112 J. H., Cuvelier, C., Graff, A., Jonson, J. E., Krol, M., Langner, J., Roberts, P., Rouil, L., Stern, R., Tarrasón, L.,  
1113 Thunis, P., Vignati, E., White, L., and Wind, P.: Evaluation of long-term ozone simulations from seven regional  
1114 air quality models and their ensemble, *Atmospheric Environment*, 41, 2083-2097,  
1115 10.1016/j.atmosenv.2006.10.073, 2007.

1116 Vautard, R., Builtjes, P. H. J., Thunis, P., Cuvelier, C., Bedogni, M., Bessagnet, B., Honoré, C., Moussiopoulos,  
1117 N., Pirovano, G., and Schaap, M.: Evaluation and intercomparison of Ozone and PM10 simulations by several

1118 chemistry transport models over four European cities within the CityDelta project, *Atmospheric Environment*,  
1119 41, 173-188, 10.1016/j.atmosenv.2006.07.039, 2007.  
1120 Vliet, V. E. a. K., P.: Impacts of roadway emissions on urban particulate matter concentrations in sub-Saharan  
1121 Africa: new evidence from Nairobi, Kenya, *Environmental Scientific letters*, 2, [https://doi.org/10.1088/1748-](https://doi.org/10.1088/1748-9326/2/4/045028)  
1122 [9326/2/4/045028](https://doi.org/10.1088/1748-9326/2/4/045028), 2007.  
1123 Voulgarakis, A., Savage, N. H., Wild, O., Carver, G. D., Clemitshaw, K. C., Pyle, J. A.: Upgrading photolysis in  
1124 the PHOTOMCAT CTM: model evaluation and assessment of the role of clouds, *Geoscientific Model*  
1125 *Development*, 2, 59-72, <https://doi.org/10.5194/gmd-2-59-2009>, 2009.  
1126 World Bank Open Data: <https://data.worldbank.org/>, access: June 2022, 2022.  
1127 WHO: WHO Air quality guidelines for particulate matter, ozone, nitrogen dioxide and sulfur dioxide, 2005.  
1128 WHO: Burden of disease from ambient air pollution for 2012, 2012.  
1129 WHO: Ambient Air Pollution: A global assessment of exposure and burden of disease, 2016.  
1130 Wild, O., Zhu, X., and Prather, J.: Fast-J: Accurate simulation of the in- and below cloud photolysis in  
1131 tropospheric chemical models., *J. Atmos. Chem*, 37, 245-282, <https://doi.org/10.1023/A:1006415919030>, 2000.  
1132 Wu, W.-S., Purser, R.J., Parrish, D.F., : Three-dimensional variational analysis with spatially inhomogeneous  
1133 covariances., *Mon. Weather Rev.*, 130, 2905–2916, [https://doi.org/10.1175/1520-](https://doi.org/10.1175/1520-0493(2002)130<2905:TDVAWS>2.0.CO;2)  
1134 [0493\(2002\)130<2905:TDVAWS>2.0.CO;2](https://doi.org/10.1175/1520-0493(2002)130<2905:TDVAWS>2.0.CO;2), 2002.  
1135 Zhang, L., Gong, S., Padro, J., and Barrie, L.: A size-segregated particle dry deposition scheme for an  
1136 atmospheric aerosol module, *Atmospheric Environment*, 35, 549-560, [https://doi.org/10.1016/S1352-](https://doi.org/10.1016/S1352-2310(00)00326-5)  
1137 [2310\(00\)00326-5](https://doi.org/10.1016/S1352-2310(00)00326-5), 2001.  
1138 Zyryanov, D., Foret, G., Eremenko, M., Beekmann, M., Cammas, J. P., D'Isidoro, M., Elbern, H., Flemming, J.,  
1139 Friese, E., Kioutsoutkis, I., Maurizi, A., Melas, D., Meleux, F., Menut, L., Moinat, P., Peuch, V. H., Poupkou,  
1140 A., Razinger, M., Schultz, M., Stein, O., Suttie, A. M., Valdebenito, A., Zerefos, C., Dufour, G., Bergametti, G.,  
1141 and Flaud, J. M.: 3-D evaluation of tropospheric ozone simulations by an ensemble of regional Chemistry  
1142 Transport Model, *Atmospheric Chemistry and Physics*, 12, 3219-3240, 10.5194/acp-12-3219-2012, 2012.

1143